

## Durham Research Online

---

**Deposited in DRO:**

**Version of attached file:**

Accepted Version

**Peer-review status of attached file:**

Peer-reviewed

**Citation for published item:**

Burton-Johnson, A and Macpherson, C G and Ottley, C J and Nowell, G M and Boyce, A J (2019) 'Generation of the Mt Kinabalu granite by crustal contamination of intraplate magma modelled by equilibrated major element assimilation with fractional crystallization (EME-AFC).', *Journal of petrology.*, 60 (7). pp. 1461-1487.

**Further information on publisher's website:**

<https://doi.org/10.1093/petrology/egz036>

**Publisher's copyright statement:**

This is a pre-copyedited, author-produced PDF of an article accepted for publication in *Journal of Petrology* following peer review. The version of record Burton-Johnson, A, Macpherson, C G, Ottley, C J, Nowell, G M Boyce, A J (2019). Generation of the Mt Kinabalu Granite by Crustal Contamination of Intraplate Magma Modelled by Equilibrated Major Element Assimilation with Fractional Crystallization (EME-AFC). *Journal of Petrology* 60(7): 1461-1487 is available online at: <https://doi.org/10.1093/petrology/egz036>

**Additional information:**

## Use policy

---

The full-text may be used and/or reproduced, and given to third parties in any format or medium, without prior permission or charge, for personal research or study, educational, or not-for-profit purposes provided that:

- a full bibliographic reference is made to the original source
- a [link](#) is made to the metadata record in DRO
- the full-text is not changed in any way

The full-text must not be sold in any format or medium without the formal permission of the copyright holders.

Please consult the [full DRO policy](#) for further details.

**Generation of the Mt Kinabalu granite by crustal contamination of intraplate  
magma modelled by Equilibrated Major Element Assimilation with Fractional  
Crystallisation (EME-AFC)**

---

Burton-Johnson, A.<sup>a\*</sup>, Macpherson, C.G.<sup>b</sup>, Ottley, C.J.<sup>b</sup>, Nowell, G.M.<sup>b</sup>, and Boyce,  
A.J.<sup>c</sup>

<sup>a</sup>British Antarctic Survey, High Cross, Madingley Road, Cambridge, CB3 0ET, UK

<sup>b</sup>Department of Earth Sciences, University of Durham, Durham, DH1 3LE, UK

<sup>c</sup>Scottish Universities Environmental Research Centre, East Kilbride, G75 0QF, UK

\*Author for correspondence

e-mail: [alerto@bas.ac.uk](mailto:alerto@bas.ac.uk)

Tel. +44 (0)1223 221284

## ABSTRACT

We present new geochemical data for the composite units of the Mount Kinabalu granitoid intrusion of Borneo and explore discrimination between crustal- and mantle-derived granitic magmas. The geochemical data demonstrate that the units making up this composite intrusion became more potassic through time. This was accompanied by an evolution of isotope ratios from a continental-affinity towards a slightly more mantle-affinity ( $^{87}\text{Sr}/^{86}\text{Sr}_i \sim 0.7078$ ;  $^{143}\text{Nd}/^{144}\text{Nd}_i \sim 0.51245$ ;  $^{206}\text{Pb}/^{204}\text{Pb}_i \sim 18.756$  for the oldest unit compared to  $^{87}\text{Sr}/^{86}\text{Sr}_i \sim 0.7065$ ,  $^{143}\text{Nd}/^{144}\text{Nd}_i \sim 0.51250$  and  $^{206}\text{Pb}/^{204}\text{Pb}_i \sim 18.721$  for the younger units). Oxygen isotope ratios (calculated whole rock  $\delta^{18}\text{O}$  of  $+6.5\text{--}9.3\text{‰}$ ) do not show a clear trend with time. The isotopic data indicate that the magma cannot be the result only from fractional crystallisation of a mantle-derived magma. Alkali metal compositions show that crustal anatexis is also an unsuitable processes for genesis of the intrusion. The data indicate that the high-K units were generated by fractional crystallisation of a primary, mafic magma followed by assimilation of the partially melted sedimentary overburden. We present a new, Equilibrated Major Element – Assimilation with Fractional Crystallisation (EME-AFC) approach for simultaneously modelling the major element, trace element, and radiogenic and oxygen isotope compositions during such magmatic differentiation; addressing the lack of current AFC modelling approaches for felsic, amphibole- or biotite-bearing systems. We propose that Mt Kinabalu was generated through low degree melting of upwelling fertile metasomatised mantle driven by regional crustal extension in the Late Miocene.

## KEY WORDS

Granite petrogenesis; Magma differentiation; AFC modelling; Oxygen isotopes; Borneo

## INTRODUCTION

Granitic intrusions form the majority of the Earth's upper continental crust and are commonly associated with precious metal deposits. Understanding their emplacement mechanisms and structure in the crust has evolved from models of slow moving diapirs to rapid, often pulsed, dyke emplacement of laterally extensive laccoliths (e.g. Wiebe, 1988; Clemens and Mawer, 1992; McCaffrey and Petford, 1997; Cruden, 1998; Wiebe and Collins, 1998; Petford and Clemens, 2000; Petford *et al.*, 2000; Vigneresse and Clemens, 2000; de Saint-Blanquat *et al.*, 2006; Vigneresse, 2006; de Silva and Gosnold, 2007; Grocott *et al.*, 2009; Horsman *et al.*, 2009). However, the processes that generate granitic melts remain ambiguous and debated (e.g. de Fátima Bitencourt *et al.*, 2017; Jagoutz and Klein, 2018).

Three potential mechanisms for producing granitic melts are widely accepted: (i) fractionation of mafic mantle derived melts, (ii) crustal anatexis, and (iii) mixing of mantle and anatectic melts. Each of these have been proposed for different plutons worldwide (e.g. Bogaerts *et al.*, 2006; Jagoutz *et al.*, 2009; Clemens and Benn, 2010; Chappell and White, 2011; Leuthold *et al.*, 2012). Distinguishing between these processes remains contentious and a fundamental challenge in igneous petrogenesis, but one that is best tackled through a comprehensive geochemical approach.

In this paper we present new geochemical data for the Mt Kinabalu pluton of Sabah in Malaysian Borneo. This is an ideal target to study granite petrogenesis because it is composed of units that are mineralogically and geochemically distinct and have ages that are well constrained by both contact relationships and U-Pb zircon dating (Cottam *et al.*, 2010; Burton-Johnson *et al.*, 2017). We show that neither crustal anatexis nor fractionation of mantle melts without crustal involvement are suitable mechanisms to generate this body. Utilising a new geochemical modelling approach we show that the intrusion's granitic magma was produced by crustal contamination of mantle derived, intra-plate magma by Assimilation and Fractional Crystallisation (AFC) processes.

## REGIONAL GEOLOGY

At 4095m elevation, Mt Kinabalu is the highest peak between the Himalayas and Papua New Guinea (Fig. 1a and 1b). The Mt Kinabalu pluton was emplaced in Sabah, NW Borneo during the late Miocene (Fig. 1c). The region has basement made up of four main components: Jurassic to Cretaceous mafic igneous rocks; Cretaceous radiolarian cherts; variably serpentinitised peridotites; and Triassic to Cretaceous rocks, previously described as crystalline basement (Reinhard and Wenk, 1951; Dhonau and Hutchison, 1965; Koopmans, 1967; Kirk, 1968; Leong, 1974; Rangin *et al.*, 1990; Omang, 1993; Swauger *et al.*, 1995; Graves *et al.*, 2000; Hutchison, 2005). These are overlain by a thick cover sequence of predominantly deep-water turbidites and related deposits (Collenette, 1965; van Hattum *et al.*, 2013) of the Cretaceous to Eocene Rajang Group (Sapulut Formation) and the Eocene to Oligocene Crocker Group (including the Trusmadi, Crocker, and Temburong Formations.)

88 The basement and cover sequence were folded and faulted during Eocene and  
89 Oligocene deformation driven by the subduction of the proto-South China Sea  
90 beneath Borneo (Taylor & Hayes 1983; Rangin & Silver 1990; Tongkul 1991, 1994;  
91 Hall 1996; Hall & Wilson 2000; Hutchison 2000). The attenuated South China  
92 continental margin collided with northern Borneo in the Early Miocene (Hall and  
93 Wilson, 2000; Hutchison, 2000; Hall and Breitfeld, 2017) triggering the Sabah  
94 Orogeny (Hutchison, 1996). The Kinabalu granite was intruded, under extensional  
95 strain, into the central Crocker Mountains in the Late Miocene (7-8 Ma; Cottam *et al.*,  
96 2010; Burton-Johnson *et al.*, 2017, 2019). The nearest contemporaneous granitic  
97 magmatism is the Capoas Granite (Fig. 1a), 600 km to the NE in Palawan (13.5 Ma,  
98 Suggate *et al.* 2013), although <5 Ma enriched basaltic to dacitic magmatism is  
99 recorded in Borneo on the Semporna Peninsula, and at Usun Apau and Linau Balui  
100 (Fig. 1a, Macpherson *et al.*, 2010; Cullen *et al.*, 2013).

101

## 102 **Field relations of the Mt Kinabalu pluton**

103

104 The Mt Kinabalu pluton was emplaced as six major granitic units (Fig. 1c, see  
105 Burton-Johnson *et al.*, 2017 for petrographic descriptions). Revised field relationships  
106 and U-Pb zircon ages have shown that the composite pluton was initially emplaced  
107 from the top down in a broadly laccolitic structure through upward deformation of the  
108 host rocks (Cottam *et al.*, 2010; Burton-Johnson *et al.*, 2017). Consequently, the  
109 oldest unit, the Alexandra Tonalite/Granodiorite ( $7.85 \pm 0.08$  Ma), lies above  
110 subsequent, larger units of the Low's Granite ( $7.69 \pm 0.07$  Ma) and the King Granite  
111 ( $7.46 \pm 0.08$  Ma). The smaller, vertical, planar Donkey Granite ( $7.49 \pm 0.03$  Ma)  
112 intruded the King Granite before the latter could fully crystallise, producing contacts

that vary between gradational and mingled. The final two porphyritic units (the Paka Porphyritic Granite,  $7.32 \pm 0.09$  Ma, and the Mesilau Porphyritic Granite,  $7.22 \pm 0.07$  Ma) deviate from the laccolith model having been emplaced laterally and around the periphery of the earlier units (Fig. 1c; Burton-Johnson *et al.*, 2017). Field evidence for the approximate volumes of the pluton's composite units (Fig. 1c, Burton-Johnson *et al.*, 2017) and the U-Pb zircon ages (Cottam *et al.*, 2010) give a total pluton volume of  $\sim 170$  km<sup>3</sup> and a total emplacement period of 0.6 Ma. This equates to an average emplacement rate of  $\sim 3 \times 10^{-4}$  km<sup>3</sup>yr<sup>-1</sup>; comparable with evidence from other plutons worldwide (de Saint Blanquat *et al.*, 2011; Menand *et al.*, 2015).

## **METHODOLOGY**

Samples were analysed from each granitic unit, from the turbidite overburden of the Crocker Formation, and from a xenolith found in the intrusion (a conglomerate within the Donkey Granite, Fig. 1). Samples were powdered by fly press and agate ball mill. Major element chemistry was obtained by XRF at Edinburgh University. Samples were dried at 1100°C, mixed with LiBO<sub>2</sub> flux and fused into glass discs for analysis (Gill, 1997). Trace element chemistry was obtained on a ThermoScientific X-Series 2 ICP-MS (Durham University). The methodology, blank, and detection limits are given in Ottley *et al.* (2003). Sample powders were dissolved using HF and HNO<sub>3</sub>, and blanks, repeated samples and the standards BHVO-1, W2 and AGV-1 analysed for calibration and QC (Ottley *et al.*, 2003). To ensure zircon dissolution, granitic samples were fused prior to crushing and dissolution. Accuracy and reproducibility were monitored using standards AGV-1, BHVO-1, and W2, and through replicate

137 analysis of Mt Kinabalu samples (Supplementary Material 1 and Burton-Johnson,  
138 2013).

139 Radiogenic isotope chemistry was obtained by Plasma Ionisation Multi-collector  
140 Mass Spectrometer (PIMMS, Durham University). Sr and Nd isotopic analyses  
141 followed the column chemistry procedures of Charlier *et al.* (2006). Whole rock  
142 powders were dissolved in HF and HNO<sub>3</sub> SpA acid and separated by column  
143 chemistry using Sr-spec resin and Hf-Nd cation resin (AG50 X-8). The lead fraction  
144 was collected in 100µl 8N HCl from the Sr columns following collection of the Nd  
145 and Sr fractions and elution of waste using 200µl 2.5N HCl. The Pb fraction was  
146 dried down, dissolved in 500µl 3% HNO<sub>3</sub>, and spiked with <sup>206</sup>Tl to correct for mass  
147 bias (Hirata, 1996). PIMMS analytical procedures are detailed in Nowell *et al.*  
148 (2003). For Nd and Sr, measured values for the NBS987 and J&M standards (±2SD  
149 error) during the same run as the samples were 0.710269 ±23 (n=35) and 0.511110  
150 ±11 (n=44) respectively. Data are corrected to the respective NBS987 and J&M  
151 standard values of 0.71024 (Thirlwall, 1991) and 0.511110 (Royse *et al.*, 1998). For  
152 Pb, measured values for the NBS981 standards ±2SD for <sup>206</sup>Pb/<sup>204</sup>Pb, <sup>207</sup>Pb/<sup>204</sup>Pb,  
153 <sup>208</sup>Pb/<sup>204</sup>Pb, <sup>207</sup>Pb/<sup>206</sup>Pb and <sup>208</sup>Pb/<sup>206</sup>Pb (n=20) are 16.9405 ±9, 15.4981 ±9, 36.7177  
154 ±23, 0.91486 ±3 and 2.1674 ±1 respectively. Data are corrected to the respective  
155 values of NBS981 of 16.9405, 15.4980, 36.7174, 0.91485 and 2.1674 (Galer, 1997).

156 Oxygen isotope ratios of mineral separates were analysed by laser fluorination  
157 (SUERC, East Kilbride). Oxygen was extracted by heating c. 1mg of sample with a  
158 laser in the presence of ClF<sub>3</sub> (Mattey and Macpherson, 1993). Oxygen was converted  
159 to CO<sub>2</sub> and isotopic ratios were analysed using a VG PRISM 3 dual inlet mass  
160 spectrometer. Results are reported as δ<sup>18</sup>O values in per mille (‰) deviations from  
161 Vienna Standard Mean Ocean Water (V-SMOW). For precision, all sample analyses



were repeated. Four analyses of the reference standards SES, GP147 and UWG2 were made each day for daily calibration, and their mean daily standard error from published isotopic values is 0.15‰ and the maximum daily standard error was 0.26‰.

Major element mineral chemistry was determined for polished thin sections using a JEOL JXA-8100 Superprobe electron microprobe (EMP) paired with an Oxford Instruments INCA energy-dispersive microanalytical system (EDS) at Birkbeck College. Analyses were performed using an accelerating voltage of 15 kV, a beam current of 10 nA, and a beam diameter of 1 µm. Calibration used standards of natural silicates, oxides, and Specpure metals, and a ZAF correction procedure was applied.  $X_{Fe^{3+}}$  ( $Fe^{3+}/Fe_{total}$ ) for individual minerals was calculated from the charge balance and stoichiometry.

## RESULTS

Data for all whole rock major and trace element geochemical analyses are presented in Table 1, whole rock isotope data and mineral separate oxygen isotope data in Table 2. Major element mineral chemistry is presented in Supplementary Material 2.

### Major and trace elements

Mineralogically the individual units that comprise the Mt Kinabalu intrusion are largely granites (Burton-Johnson *et al.*, 2017). Geochemically the Alexandra Tonalite/Granodiorite and Low's Granite are diorites and later units are granodiorites and syenodiorites (Fig. 2a). Our analyses show a similar range in compositions to previous analyses by Vogt and Flower (1989), but coupling geochemical data with

mapping (Burton-Johnson *et al.*, 2017) and geochronological data (Cottam *et al.*, 2010) allows us to recognise a more refined structure of units (Fig. 2). All units are sub-alkalic and enriched in potassium, with the Alexandra Tonalite/Granodiorite and Low's Granite classified as high-K calc-alkaline and the later units as shoshonitic (Fig. 2b). While Alexandra Tonalite/Granodiorite is weakly peraluminous all subsequent units are metaluminous. Amphibole chemistry is calcic and dominantly magnesio-hornblende in classification (Fig. 3).

Trace element ratios show that Kinabalu rocks display uniform, relative depletion in Nb and Ta, and enrichment of K and Pb. Such signatures are similar to continental crust or arc magmatism. Chondrite normalised REE plots (Fig. 4) show elevated LREE/HREE and concave middle to heavy REE. Each unit displays a negative Eu anomaly.

## **Radiogenic Isotopes**

The Alexandra Tonalite/Granodiorite ( $^{87}\text{Sr}/^{86}\text{Sr}_i \sim 0.7076$ ;  $^{143}\text{Nd}/^{144}\text{Nd}_i \sim 0.51247$  ( $\epsilon\text{Nd} -3.19$ );  $^{206}\text{Pb}/^{204}\text{Pb}_i \sim 18.754$ ) is consistently displaced farther from mantle compositions than the younger intrusive units ( $^{87}\text{Sr}/^{86}\text{Sr}_i \sim 0.7066$ ,  $^{143}\text{Nd}/^{144}\text{Nd}_i \sim 0.51251$  ( $\epsilon\text{Nd} -2.39$ ) and  $^{206}\text{Pb}/^{204}\text{Pb}_i \sim 18.724$ ). Likewise, the Mt Kinabalu isotopes are displaced to more radiogenic Sr and Pb, and less radiogenic Nd than uncontaminated, mantle-derived basalts from Borneo and the adjacent South China Sea (Fig. 5a, Chen *et al.*, 2008; Wang *et al.*, 2008; Macpherson *et al.*, 2010; Cullen *et al.*, 2013). Isotopically, Kinabalu rocks (Fig. 5) are more similar to Mesozoic granites from the South China Sea (Yan and Shi, 2009; Yan *et al.*, 2010), the Capoas granite of Palawan (Encarnación and Mukasa, 1997; Burton-Johnson, 2013), and

the least radiogenic rocks from Vietnam, Hong Kong and Yunnan (Thuy *et al.*, 2004). Pb data for the region's magmatism, including Mt Kinabalu, diverges from the Northern Hemisphere Reference Line (NHRL) towards an enriched mantle (EMII) composition (Fig. 5b, Zindler and Hart, 1986), as noted by previous authors (Hoang *et al.*, 1996; Yan *et al.*, 2008).

## Oxygen Isotopes

$\delta^{18}\text{O}$  values range between +9.4 and +10.3‰ for quartz, and between +6.6 and +8.2‰ for hornblende (Fig. 6). By analysing both hornblende and quartz, post-crystallisation alteration of the oxygen isotope composition can be assessed. Equilibration at magmatic temperatures produces lower and more restricted  $\Delta^{18}\text{O}_{\text{quartz-hornblende}}$  isotope values (where  $\Delta^{18}\text{O}_{\text{quartz-hornblende}} = \delta^{18}\text{O}_{\text{quartz}} - \delta^{18}\text{O}_{\text{hornblende}}$ ) than lower temperature equilibration with altering fluids. Measured  $\Delta_{\text{quartz-hornblende}}$  values are equivalent to temperatures of 650-1100°C (Fig. 6; Lackey *et al.*, 2008, and references therein). Within error (Fig. 6), this range is reasonable for mineral-mineral equilibrium in felsic magma containing hornblende, which, at 200 MPa vapour-saturated conditions, should be stable below 960°C ( $\pm 10^\circ\text{C}$ ) to a solidus temperature 675° ( $\pm 25^\circ\text{C}$ , Naney, 1983).

Assuming that  $\delta^{18}\text{O}$  values of all minerals represent magmatic conditions, we can estimate magmatic  $\delta^{18}\text{O}$  values for all the other minerals by employing  $\Delta_{\text{mineral-hornblende}}$  values (Lackey *et al.*, 2008, and references therein) for the temperatures determined by  $\Delta_{\text{quartz-hornblende}}$  thermometry. A  $\delta^{18}\text{O}$  for the bulk magma from which each sample crystallised can then be calculated through mass balance using: 1. the estimated magmatic  $\delta^{18}\text{O}$  of each phase, and 2. the modal proportions of each phase in each

sample (as measured by point-counting, Burton-Johnson *et al.*, 2017). We used this methodology for determining whole rock  $\delta^{18}\text{O}$  in preference to bulk sample analysis of  $\delta^{18}\text{O}$  due to the slow diffusion rate of oxygen in hornblende (Farver and Gilotti, 1985). This method thus allows an estimate of magmatic  $\delta^{18}\text{O}$  without the influence of meteoric water alteration, which would otherwise result in sub-solidus  $\delta^{18}\text{O}$  alteration of phases possessing a faster diffusion rate (e.g. quartz and feldspar).

## DISCUSSION

The only previous geochemical study of Mt Kinabalu (Vogt and Flower, 1989) concluded that rocks of the Alexandra Tonalite/Granodiorite unit (then termed the Biotite Quartz Monzodiorite by Vogt and Flower, 1989), represented the most primitive magma in the intrusion and were produced by remelting of underplated basalt. It was proposed that all other units (collectively referred to as Hornblende Quartz Monzonite) were the result of further crustal contamination of the Biotite Quartz Monzodiorite. Our isotopic data demonstrate that the Alexandra unit has the most “crustal” isotopic ratios and so this relationship with the rest of the intrusion is unlikely. Furthermore, the model developed by Vogt and Flower (1989) assumed that the Alexandra unit was at the core of a nested diaper and so represented the youngest unit of Kinabalu. Mapping and U-Pb geochronology of zircon has subsequently demonstrated that the intrusion is layered with the Alexandra unit being its oldest component (Fig. 1; Cottam *et al.*, 2010).

Granitic melts can be derived through fractionation of mantle-derived melts, with or without crustal assimilation (assimilation and fractional crystallisation, AFC), or through partial melting of crustal lithologies (crustal anatexis) (e.g. Bogaerts *et al.*,

2006; Jagoutz *et al.*, 2009; Clemens and Benn, 2010; Chappell and White, 2011; Leuthold *et al.*, 2012; Jagoutz and Klein, 2018). We combine our new geochemical data with mapping and geochronological constraints to evaluate the likelihood that Mt Kinabalu magma was generated by these three mechanisms.

## **Crustal anatexis**

Potential crustal sources for Mt Kinabalu magma are: (i) ophiolitic basement, (ii) turbidite sediments, (iii) older felsic continental crust beneath Sabah (previously postulated by Macpherson *et al.* 2010), (iv) continental crust under-thrust beneath Borneo during the final stages of Proto South China Sea subduction, or (v) gabbroic lower crust (Vogt and Flower, 1989). The isotopic ratios of Mt Kinabalu rocks are sufficiently displaced from mantle compositions for us to discount an origin solely from melting ophiolitic basement. However, the radiogenic isotopes cannot conclusively rule out the other possibilities, particularly as the turbidite sediments are variable in their composition, while the monzogranites and tonalites dredged from attenuated continental crust of the South China Sea share similar isotopic signatures to Mt Kinabalu (Fig. 5).

To evaluate the feasibility of producing Mt Kinabalu magma by crustal anatexis, we compiled data for melting experiments on igneous and sedimentary rocks and their metamorphic equivalents (Fig. 7). These experiments were conducted on a wide range of compositions over a range of temperatures, pressures, water contents and redox conditions. The alkali metal compositions show that the different protoliths produce melts with distinctive compositional ranges, regardless of the degree of melting (Fig. 7). Melting of a sedimentary protolith generates peraluminous melt compositions with

high K/Na and very low Ca/Na ratios, and with very restricted ratios of  $\text{Al}/(\text{Na} + \text{K}) : \text{Al}/(\text{Ca} + \text{Na} + \text{K})$  (Fig. 7). Melting felsic crustal protoliths yield similar compositions but tend to have even higher and more scattered K/Na (Fig. 7a). None of these protoliths generates comparable melts to the largely metaluminous, high-Ca/Na and high K/Na samples from Mt Kinabalu.

Partial melts of basaltic lithologies range from peraluminous to metaluminous (~90% are peraluminous) and their  $\text{Al}/(\text{Na} + \text{K}) : \text{Al}/(\text{Ca} + \text{Na} + \text{K})$  ratios can resemble Kinabalu rocks (Fig. 7b). However, their generally low K/Na ratios and consistently low Ca/Na ratios (Fig. 7a) suggest that these are also unlikely sources for the Kinabalu magmas. This corroborates our earlier inference made on the basis of isotopic ratios. Only melts derived from exceptionally Ca-rich and Na- and K-deficient basaltic amphibolites (Wolf and Wyllie, 1994) possess Ca/Na ratios as high as Kinabalu (Fig. 7a), but these are strongly peraluminous with exceptionally high  $\text{Al}/(\text{Na} + \text{K})$  and K/Na much lower than the Mt Kinabalu granitoids. This also means that any mixture of such high Ca/Na melt with high K/Na sources would remain peraluminous, dissimilar to Mt Kinabalu. Consequently, melts derived solely from crustal anatexis, be they from a single source or any likely mixtures (including the mafic lower crust), cannot reproduce the major element composition of Mt Kinabalu, or other metaluminous and intermediate to high Ca/Na and K/Na magmatism.

Prouteau *et al.* (2001) suggested that the Kinabalu intrusion is adakitic. We dispute an origin for Mt Kinabalu magma through melting of subducted oceanic crust as the major element compositions of partial melts from hydrous, basaltic amphibolites (Winther and Newton, 1991; Sen and Dunn, 1994; Rapp and Watson, 1995) are distinct from the Kinabalu rocks (Fig. 7). Neither our data nor that from preceding studies (Vogt and Flower, 1989) possess the distinctive trace element signatures of

these putative slab melts (Defant and Drummond, 1990). Furthermore, the radiogenic isotope ratios of all Kinabalu units lie outside the fields of most ocean floor basalts, including the South China Sea (Fig. 4). Therefore, we dismiss this as a possible origin for the Kinabalu magmas.

### **Fractional crystallisation of mantle-derived basalt**

Experimental petrology demonstrates the potential for fractional crystallisation of mafic magmas to produce granitic melts (e.g. Grove *et al.*, 2003; Alonso-Perez *et al.*, 2009; Nandedkar *et al.*, 2014; Müntener and Ulmer, 2018). There is no evidence in the immediate vicinity of Mt. Kinabalu for contemporaneous mafic magmatism, but Neogene basaltic volcanism occurred in other north Borneo locations, such as Semporna, Usun Apau and Linau Balui (Fig. 1a, Macpherson *et al.*, 2010; Cullen *et al.*, 2013), with evidence of differentiation to more felsic compositions of these locations. However, fractional crystallisation alone cannot be responsible for the range of Kinabalu magma compositions. The isotope ratios of Sr, Nd and Pb are all substantially displaced from those of Neogene basalt from Borneo, other than those identified as having experienced substantial crustal contamination (Fig. 5; Macpherson *et al.*, 2010). There is also significant variation between the different Kinabalu units, without large contrasts in trace element ratios, which are more readily reconciled with open-system behaviour in the crust. This is further suggested by the large range of oxygen isotope ratios, which include values for mafic phases, such as hornblende, that are substantially higher than those that would be expected to be in equilibrium with mantle-derived magma (Mattey *et al.*, 1994; Macpherson and Mattey, 1998; Lackey *et al.*, 2008). Therefore, we conclude that the isotopic diversity of the Mt Kinabalu

granitic intrusion cannot be explained by the fractionation of mantle-derived basalt alone, and instead requires open-system processes in the Borneo crust.

### **Crustal contamination of magma: Equilibrated Major Element – Assimilation with Fractional Crystallisation (EME-AFC)**

To model open-system behaviour for the various geochemical properties considered here we developed an incremental major element AFC model of Equilibrated Major Element AFC (EME-AFC). This was undertaken because the thermodynamic model MELTS (Ghiorso and Sack, 1995) is not recommended for felsic or intermediate systems, and neither MELTS or rhyolite-MELTS (which can model high-silica systems, Gualda *et al.*, 2012) can model hydrous magmatic systems involving substantial hornblende or biotite fractionation. The Magma Chamber Simulator (Bohrson *et al.*, 2014) utilises MELTS, so is also unable to model systems involving significant fractionation of hydrous phases. Additionally, mass balance equations do not reflect the changing compositions of mineral phases in response to the geochemical evolution of the magma. Instead we developed EME-AFC modelling, which employs two-component major element partition coefficients ( $K_D^{X,Y} = (X^{Min} \cdot Y^{Liq}) / (Y^{Min} \cdot X^{Liq})$ ), where X and Y are elements in a single mineral phase (<sup>Min</sup>) in equilibrium with a liquid (<sup>Liq</sup>). This allows simultaneous modelling of major elements by EME-AFC, and trace elements, radiogenic isotopes, and oxygen isotopes by recognised methods (DePaolo, 1981).

The major element component of EME-AFC is similar to that of Grove and Donnelly-Nolan (1986) in which the Fe-Mg and Ca-Na compositions of the fractionating phases equilibrate with the evolving magma. This involved calculating the Fe-Mg and Ca-Na



361 phase compositions using two-component major element partition coefficients  
 362 ( $K_D^{Fe,Mg} = (Fe^{Min} \cdot Mg^{Liq}) / (Mg^{Min} \cdot Fe^{Liq})$  and  $K_D^{Ca,Na} = (Ca^{Min} \cdot Na^{Liq}) / (Na^{Min} \cdot Ca^{Liq})$ ) and  
 363 solving for successive increments of fractionation ( $F$ ). We broadened this approach to  
 364 a larger number of phases, equilibrating more elements and calculating the  
 365 concentrations of all major and minor elements in each phase. Assimilation is  
 366 modelled at each increment by binary mixing for the major elements according to a  
 367 user-determined rate,  $r$  (the mass assimilated / mass crystallised), which is the  
 368 parameter in AFC modelling describing the ability of magma to assimilate crust  
 369 (DePaolo, 1981; Reiners *et al.*, 1995). The formulae for each phase and the sites into  
 370 which elements can substitute are determined from Deer *et al.* (1992) and the  
 371 valency of each element. The Fe-Mg, Al-Si and K-Na partition coefficients (Table 3)  
 372 are determined from experimental data (Grove *et al.*, 2003; Alonso-Perez *et al.*,  
 373 2009; Nandedkar *et al.*, 2014). Note that, unlike trace element partition coefficients  
 374 (Supplementary Material 6), two-component major element partition coefficients have  
 375 narrow ranges of values (Table 3). Consequently, as in the “Crustal anatexis” section,  
 376 our subsequent discussion of the EME-AFC modelling focuses on the major elements.  
 377 Plagioclase fractionates as  $((K,Na)_{1-(x-1)}(Mg+Mn+Ca)_{x-1})_1((Fe+Al)_x, Si_{4-x})_4O_8$  and its  
 378 equilibrium with the coexisting evolving liquid is determined by the two-component  
 379 distribution coefficient  $K_D^{Al,Si} = Al^{Plag}Si^{Liq} / Si^{Plag}Al^{Liq}$ . The Al-Si distribution is used in  
 380 preference to the Ca-Na distribution as  $K_D^{Al,Si}$  in plagioclase is far less variable than  
 381  $K_D^{Ca,Na}$  (1.8-4.2, compared to 0.6-16.2, Grove *et al.*, 2003; Alonso-Perez *et al.*,  
 382 2009; Nandedkar *et al.*, 2014). The Na-K distribution is calculated from  $K_D^{K,Na} =$   
 383  $K^{Plag}Na^{Liq} / Na^{Plag}K^{Liq}$ . Fe substitutes for Al, and Mg, and Mn substitute for Ca in  
 384 proportions determined empirically from the Mt Kinabalu mineral chemistry  
 385 (Supplementary Material 3). Hornblende fractionates as  $(Na,K)_0-$

$_{1}\text{Ca}_2((\text{Mn},(\text{Mg},\text{Fe})),(\text{Ti}(\text{Al},\text{Si})))_{13}\text{O}_{22}(\text{OH})$ , and its equilibrium with silicate liquid is determined using the Fe-Mg and Al-Si two-component partition coefficients:  $K_D^{\text{Fe,Mg}} = \text{Fe}^{\text{Hb}}\text{Mg}^{\text{Liq}}/\text{Mg}^{\text{Hb}}\text{Fe}^{\text{Liq}}$  and  $K_D^{\text{Al,Si}} = \text{Al}^{\text{Hb}}\text{Si}^{\text{Liq}}/\text{Si}^{\text{Hb}}\text{Al}^{\text{Liq}}$ . Orthopyroxene and clinopyroxene fractionate as  $((\text{Ca},\text{Na}),(\text{Mn},(\text{Mg},\text{Fe})))_2(\text{Si},(\text{Ti},\text{Al}))_2\text{O}_6$  and use the Fe-Mg and Al-Si mineral-melt distribution coefficients:  $K_D^{\text{Fe,Mg}} = \text{Fe}^{\text{Opx}}\text{Mg}^{\text{Liq}}/\text{Mg}^{\text{Opx}}\text{Fe}^{\text{Liq}}$ , and  $K_D^{\text{Al,Si}} = \text{Al}^{\text{Cpx}}\text{Si}^{\text{Liq}}/\text{Si}^{\text{Cpx}}\text{Al}^{\text{Liq}}$ . Biotite fractionates as  $(\text{K},\text{Na})_2(((\text{Mg},\text{Fe})\text{Ti})\text{Mn})_{4-6},(\text{Al},\text{Si})_{8-10})_{14}\text{O}_{20}(\text{OH})_4$ , and equilibrates with the liquid using  $K_D^{\text{Al,Si}} = \text{Al}^{\text{Plag}}\text{Si}^{\text{Liq}}/\text{Si}^{\text{Plag}}\text{Al}^{\text{Liq}}$ . Both olivine and garnet equilibrate using Fe-Mg mineral-melt partition coefficients and fractionate as  $((\text{Mg},\text{Fe}),\text{Ca},\text{Mn})_2(\text{Si},\text{Al},\text{Ti})\text{O}_4$ , and  $(\text{Mg},\text{Fe})_3\text{Al}_2\text{Si}_3\text{O}_{12}$ , respectively. Major and minor element concentrations not determined by two-component partition coefficients or stoichiometry are calculated for each phase by mean or linear regression correlations with other major elements in the mineral separate data (Supplementary Material 3). These calculations along with a detailed explanation of the major element modelling are presented in Supplementary Material 3 and Supplementary Material 4, as well as the EME-AFC modelling spreadsheet (Supplementary Material 5).

The trace element and isotopic components of EME-AFC are calculated at each increment using the AFC equations of DePaolo (1981). Trace element partition coefficients are compiled and calculated from the GERM database (<https://earthref.org/KDD/>) except quartz (Nash and Crecraft, 1985). Where reasonable, absent REE partition coefficients are interpolated. The compiled and calculated partition coefficients and their references are provided in Supplementary Material 6. Partial melting of the assimilant prior to assimilation in the melt is incorporated for the trace elements by batch modal melting with user-determined assimilant mineralogy and melt fraction ( $F_{\text{Assimilant}}$ ).

To accommodate the changing nature of element partitioning during magmatic differentiation, EME-AFC employs four intervals of SiO<sub>2</sub> content representing melt compositions of basalt, basaltic andesite, andesite and rhyolite (note that the basaltic andesite starting material for the Mt Kinabalu models below is more evolved than the basaltic interval). Each interval uses appropriate major and trace element partition coefficients (Table 3). The two-component major element partition coefficients used in the EME-AFC model do not correlate with melt SiO<sub>2</sub> except for the Al-Si coefficient of plagioclase, which changes in the model at 57 and 63 wt.% SiO<sub>2</sub>. In addition to the magmatic composition, at each increment the composition of the bulk cumulate assemblage, the total fraction of melt remaining in the system, and the total ratio of the mass of assimilated material to the initial magma mass ( $\rho$ ) are calculated. To constrain the fit of the model through trial and error, the sum of the differences squared ( $\sum D^2$ ) for the major elements of the model and target composition is also calculated.

Oxygen isotope fractionation between coexisting phases varies with temperature. Multivariate linear regression of experimental fractionation data for experimental conditions of 700-1300°C, 0-11% H<sub>2</sub>O and 7-12 kbar, shows that melt SiO<sub>2</sub> contents correlate strongly with temperature (Fig. 8), moderately with H<sub>2</sub>O but do not correlate with pressure (respective p-values of  $6 \times 10^{-13}$ , 0.02 and 0.7). Thus, we derived an empirical relationship between SiO<sub>2</sub> and temperature ( $T = -19SiO_2 + 2050$ ,  $R^2 = 0.75$ ,  $\pm 62^\circ\text{C}$  at 1SD). This allows the temperature, resultant  $\Delta_{\text{Mineral-Melt}}$ ,  $\delta^{18}\text{O}$  of the fractionating assemblage, and  $\delta^{18}\text{O}$  of the magma to be calculated at each model increment.

Each potential fractionating phase has specific effects on the major element, trace element, and isotopic composition of the evolving melt. This means that, in

comparison with modelling geochemical properties in isolation, EME-AFC greatly limits the range of possible fractionating assemblages that can generate a target composition.

EME-AFC has specific advantages over existing AFC models: the ability to model felsic systems and those dominated by the fractionation of hydrous mineral phases (biotite and hornblende); simultaneous modelling of major and trace elements, and radiogenic and stable isotopes; control of the fractionating system and its parameters allows exploration of each parameter or input's effects on the liquid line of descent; and, importantly, the effects of pressure, water content and oxidation state of the system are accounted for by calibrating the model to the specific mineral chemistry of the system under consideration. In addition, the EME-AFC model is run within a standard spreadsheet, without the requirement for specialist software or specific operating systems.

#### **Evaluation of EME-AFC modelling**

EME-AFC modelling was developed to address the absence of AFC modelling solutions for felsic systems involving substantial amphibole or biotite fractionation. To validate this approach we compared the outputs of EME-AFC with those of Rhyolite-MELTS (Gualda *et al.*, 2012) for fractional crystallisation models of two discrete starting compositions: a Mid-Ocean Ridge Basalt (Allan *et al.*, 1989) and a basalt from Borneo (Macpherson *et al.*, 2010).

The detailed comparison (Supplementary Material 7) shows that EME-AFC broadly reproduces the liquid lines of descent (LLD) calculated by Rhyolite-MELTS (Fig. 9). For both starting compositions the largest discrepancy results from Rhyolite-MELTS fractionating high-Al clinopyroxene ( $>13.5$  wt. %  $\text{Al}_2\text{O}_3$ ) below  $1075^\circ\text{C}$ . Due to the relationship of Al and Si in the fractionating phase compositions (Table 3), this affects

Si as well as Al evolution. Consequently, remaining melt fractions are smaller in the Rhyolite-MELTS models for the same SiO<sub>2</sub> concentration in EME-AFC. This also influences the apparent LLD for all major elements compared with SiO<sub>2</sub>. However, neither suite shows evidence for the presence of high-Al pyroxene (Allan *et al.*, 1989). Pyroxenes in mafic lavas are expected to contain Al<sub>2</sub>O<sub>3</sub> concentrations <9 wt. %, and even lower concentrations are expected for metaluminous or MORB basalts similar to those modelled (Le Bas, 1962; Nisbet and Pearce, 1977). Thus, the suitability of the calculated Rhyolite-MELTS fractionating assemblage is ambiguous, whilst the EME-AFC clinopyroxene Al<sub>2</sub>O<sub>3</sub> compositions more similar to the expected mineral chemistries of the settings modelled (Le Bas, 1962; Nisbet and Pearce, 1977).

#### **EME-AFC modelling of Mt Kinabalu**

A Linau Balui basaltic andesite sample (LB85, Cullen *et al.*, 2013) was chosen as the initial melt. This is the most local basalt for which a comprehensive major element, trace element, and radiogenic isotope dataset was available. The  $\delta^{18}\text{O}$  value of LB85 is not known but the primary melts can be assumed to have a value of +5.5‰ due to the limited variation magma derived from the mantle ( $5.5 \pm 0.35\text{‰}$ , Matthey *et al.*, 1994; Macpherson and Matthey, 1998). Metasedimentary xenoliths are the only recorded field evidence for crustal assimilation at Mt Kinabalu (Vogt and Flower, 1989; Burton-Johnson, 2013). Thus a constant elemental and isotopic composition from a metamorphosed conglomerate xenolith found within the Donkey Granite (Fig. 5) was used as the assimilant in the initial models.

Applying the model to the most voluminous unit of Mt Kinabalu, the King Granite, most of the mineral chemistries (Fig. 10) and chemical variation of the pluton can be generated through EME-AFC modelling with the exceptions of K and Na. Regardless

of the fractionating assemblage and degree of assimilation, the high-K chemistry of Mt Kinabalu cannot be replicated by assimilation of the meta-conglomerate xenolith (Fig. 11, Model 1). Experimental petrology has shown that partial melts of metasediments develop higher K than their protoliths (Fig. 7, Le Breton and Thompson, 1988; Vielzeuf and Holloway, 1988; Douce and Johnston, 1991; Gardien *et al.*, 1995; Montel and Vielzeuf, 1997). From these studies, the biotite, plagioclase, and quartz (BPQ) starting material for the melting experiments of Gardien *et al.* (1995) most closely resembles the mineralogy and chemistry of the meta-conglomerate. Incorporating this melt composition in to the EME-AFC model replicates the sense of K-enrichment required for the Alexandra unit (Fig. 11a, Model 2). However, the higher K-enrichment of the majority of units at Mt Kinabalu cannot be reproduced by this assimilant chemistry (Fig. 11a, Model 2) and the Na compositions of the Mt Kinabalu intrusive rocks are poorly reproduced (Fig. 11b, Model 2).

Increasing the modelled K<sub>2</sub>O concentration of the BPQ assimilant further shows that the K<sub>2</sub>O composition of Mt Kinabalu requires the assimilant to contain up to 12 weight % K<sub>2</sub>O. Despite the range of protolith compositions, degrees of melting, and melt conditions of the compiled data for melting experiments (as used in Fig. 7), the highest K<sub>2</sub>O concentration in the partial melt was 7.7 weight % from a metapelite (Douce and Johnston, 1991). Consequently, it is unlikely that the K-enrichment of Mt Kinabalu results from assimilation alone.

Instead, the simplest resolution to the offset from observed alkali contents is to postulate a wider range of precursor K-contents in the initial melts. A potential, contemporaneous analogue for such heterogeneity can be found in central Borneo. At 8 Ma, coincident the formation of the Mt Kinabalu intrusion, minette dykes were

emplaced at Linhaisai (Fig. 1a) as a result of low degree melting of a metasomatised, fertile mantle source (Bergman et al., 1988). These possess K<sub>2</sub>O contents ranging from 2.15 to 6.30 wt.% in relatively low silica melts (Fig. 11a). These same minettes also possess relatively low Na contents compared to Neogene basalts from Borneo (Fig. 11b). It is unlikely that the volume of magma, or the heat to generate substantial crustal melting at Kinabalu could be produced from a phase of minette-style magmatism. However, the occurrence of contemporaneous high-K, low-Na magmatism suggests that the mantle beneath Borneo may contain substantial enrichment that could generate mafic precursors of a composition between that of minette and the mafic, intraplate magma inferred for Semporna and Linau Balui (Macpherson et al., 2010; Cullen et al., 2013). Increasing the primary magma K<sub>2</sub>O to 2.5 wt. % and reducing the primary magmatic Na<sub>2</sub>O from to 2.1 wt. % generates metaluminous melts with alkali metal compositions similar to Mt Kinabalu (Fig. 11b and 11c, Model 3).

The range of the King Granite compositions (including major and trace elements, and isotopes) can be modelled by contamination of the modified primary melt (2.1 % Na<sub>2</sub>O, 2.5% K<sub>2</sub>O) by a partial melt of the meta-conglomerate. In the absence of partial melt data for the meta-conglomerate xenolith, this was simulated using the major element composition of the BPQ partial melt used in Model 2 (Fig. 11, Gardien *et al.*, 1995) and the analysed trace elements of the xenolith, modelled to the same degree of partial melting as the BPQ melting experiment ( $F_{\text{Assimilant}} = 0.09$ ).

The King Granite compositions are generated through the bulk cumulate fractionation of: 42-47% plagioclase, 14-17% clinopyroxene, 14-17% orthopyroxene, 18-20% hornblende, 0.5% apatite, 1.5% magnetite, 3.5% ilmenite, and 0.01% zircon (Fig. 12; Table 4). A  $\delta^{18}\text{O}$  value of +10‰ is required for the assimilant, which is suitable value

for this siliclastic sedimentary lithology (Magaritz *et al.*, 1978). The degree of fractionation,  $F$  (the fraction of melt remaining) is 0.54-0.66, while the required assimilation rate,  $r$  (mass assimilated / the mass crystallised at each increment of  $F$ ) is 0.4-0.57, resulting in a value for  $\rho$  (the total ratio of the mass of assimilated material to the initial magma mass) of 0.23-0.25.

Although energy constrained AFC modelling (EC-AFC, Spera and Bohrsen 2001) is unable to model major elements, it can be used to determine thermodynamic constraints for our model. EC-AFC thus indicates that  $r$  values of 0.4-0.8 are reasonable for our system given the proposed input chemistries, pre-emplacement assimilation at mid-crustal depths, and temperatures of basaltic magma. Thermodynamic modelling of AFC processes has shown that  $r$  is variable during magmatic evolution (Reiners *et al.*, 1995) and, thus, the EME-AFC model (Supplementary Material 5) can accommodate variable  $r$ . However, in the interest of not overcomplicating the Mt Kinabalu models and presenting the EME-AFC methodology here for the first time,  $r$  is treated as a constant in this scenario.

Modelling the chemistries of the remaining units indicates that similar conditions could produce the other units. However, slight differences in chemistry indicate the broad evolution of the intrusion through its emplacement. The compositional range of the Donkey Granite, Paka Porphyritic Granite and Mesilau Porphyritic Granite are similar to the King Granite (Fig. 12) so can be replicated by similar EME-AFC parameters but with variations in the degree of fractionation ( $F = 0.5$ -0.74),  $r$  (0.36-0.66), and  $\rho$  (0.2-0.25). This is more marked for the less evolved compositional range of the earlier Low's Granite, which reflects significantly lower degrees of fractionation ( $F = 0.72$ -0.78). Despite this, isotopic ratios of the Low's Granite are similar to those of the more evolved units, suggesting a higher assimilation rate ( $r =$



0.65-0.73,  $\rho = 0.16-0.21$ ). Likewise, a similar fractionating assemblage can also produce the compositional range of the earliest unit, the Alexandra Tonalite/Granodiorite ( $F = 0.59-0.73$ ), but also requires a high rate of assimilation ( $r = 0.56-0.72$ ,  $\rho = 0.22-0.29$ ) and either no K-enrichment of the primary magma or more complete melting of the assimilant (Fig. 10a). Alexandra also requires a higher  $^{207}\text{Pb}/^{204}\text{Pb}$  ratio in the assimilant than other units (Fig. 12), indicating isotopic heterogeneity in the assimilant. The assimilation rate,  $r$ , in these two oldest units is higher than those that follow but within the range of values predicted by EC-AFC. The subsequent decrease in  $r$  may reflect the reduced fertility of the assimilant following early intrusive episodes. As the source, assimilant, and fractionating assemblages are similar for all units, this reduction in assimilation rate and the degree of fractionation may have been the primary cause of geochemical heterogeneity in the Mt Kinabalu intrusion.

Due to the pluton's exceptional vertical exposure, the contacts and composite unit volumes can be constrained (Fig. 1, Burton-Johnson *et al.*, 2017). Combining this with the outputs from the EME-AFC model allows us to estimate the volume of mantle-derived magma emplaced into the crust and the volume of crust assimilated. The total pluton volume ( $V_p$ ) can be expressed as:

$$V_p = V_0 - V_c + V_a$$

[Eq. 1]

Where  $V_0$  is the primary magma volume,  $V_c$  is the volume of fractionated material and  $V_a$  is the volume of assimilated material. If  $V_c = (1-F)V_0$  and  $\rho = V_a/V_c$  then:

$$V_0 = (V_p + 1 - F)/(\rho + 1)$$

[Eq. 2]

585 Allowing a conservative 20% error in the volume estimation of the composite units,  
586 the 140-210 km<sup>3</sup> total pluton volume can be generated by 115-176 km<sup>3</sup> of primary  
587 magma and 25-43 km<sup>3</sup> of assimilated crust.

#### 589 **Nature of the crustal contaminant**

590  
591 As shown by EME-AFC modelling, partial melts of the conglomerate xenolith are a  
592 suitable analogue for the crustal contaminant required to generate the chemical  
593 heterogeneity of intrusive units at Mt Kinabalu. Further insight into the nature of the  
594 contaminating crust can be gained by comparing the inherited zircon population of Mt  
595 Kinabalu (Cottam *et al.*, 2010) to the detrital zircon populations of the regional  
596 sedimentary units (Fig. 13. van Hattum *et al.*, 2013). The Mt Kinabalu zircon  
597 population has a prominent inherited population with ages of 96 to 147 Ma, with rare,  
598 older Mesozoic ages and very few Palaeozoic or Precambrian Ages (Fig. 13). This  
599 contrasts with zircon populations hosted in the region's deep-water turbidite deposits  
600 of the Oligocene units of the Crocker Formation and the Eocene Sapulut and  
601 Trusmadi Formations, which each have a substantial population of early Mesozoic  
602 and Palaeozoic zircons, with or without notable Precambrian peaks (Fig. 13). The  
603 Upper Eocene unit of the Crocker Formation displays a very similar distribution of  
604 inherited zircon age to Mt Kinabalu (Fig. 13) and, therefore, represents the most likely  
605 local, siliclastic source of the xenolith and the contaminant of the magma that  
606 constructed the pluton.

#### 608 **Origin of the magmatism**

610 Mt Kinabalu is isolated from any contemporaneous mafic or felsic magmatism.  
611 Intraplate basalts and andesites from the Semporna peninsula (Fig. 1a) are the closest  
612 occurrence of magmatism but are younger than Kinabalu and appear to have been  
613 generated under lithosphere that was previously thinned by subduction between the  
614 Celebes and Sulu seas (Macpherson *et al.*, 2010). The Semporna magmatism may  
615 also be associated with other younger sites in central, northern Borneo, such as Usun  
616 Apau and Linau Balui (Cullen *et al.*, 2013), and possibly as far afield as Niut in  
617 western Borneo (Harahap, 1994); but the difference in ages of these events suggests  
618 there is no direct link with Mt. Kinabalu.

619 The only contemporaneous magmatism on the island is the Linhaisai minette in  
620 central Borneo (Fig. 1a) for which K-Ar dating of phlogopite ( $7.8 \pm 0.3$  Ma, Bergman  
621 *et al.*, 1988) gives almost identical ages to U-Pb dating of Kinabalu zircon (7.22-7.85  
622 Ma, Cottam *et al.*, 2010). As discussed above, the large distance between these  
623 suggest it is unlikely that they are part of the same magmatic system. However, the  
624 emplacement of two magmatic bodies, each requiring an input of primitive magma  
625 from an enriched mantle source, suggests that regional controls on mantle melting  
626 may have operated at this time.

627 Structural and Anisotropic Magnetic Susceptibility data (Burton-Johnson *et al.*,  
628 2019) indicate that Mt Kinabalu was emplaced into a zone of NNW-SSE extension,  
629 possibly the result of SE-directed slab rollback during Celebes Sea subduction to  
630 the SE (Cottam *et al.*, 2013; Hall, 2013). Extension of the crust may have provided  
631 pathways through which relatively low-degree partial melts from enriched mantle  
632 could intrude and heat the crust, allowing generation of a body composed of both  
633 mantle and crustal melts. If extension was sufficient then lithospheric thinning may  
634 have resulted in further mantle upwelling, enhancing the degree of melting and the

volume of melt produced at Mt Kinabalu. The Linhaisai minette was emplaced as a series of dykes with a broad northerly trend (Bergman *et al.*, 1988), suggesting there was also extension in central Borneo at this time. The Linhaisai minette dykes represent a more restricted event with a lower degree of partial melting, which is suggested not only by its restricted, preserved volume but also by its silica-undersaturated composition. Such magmatism would transport limited heat into the crust, which is consistent with the lack of evidence for crustal contamination here (Bergman *et al.*, 1988). Taken together, the two localities are consistent with an origin as intraplate, mafic magmatism. The major distinction is that at Mt Kinabalu there was a sufficient flux of magma, and heat, to promote melting of, and contamination by, the local upper crust.

#### **Distribution of the EME-AFC Model**

For application to other studies, a user-friendly spreadsheet of the EME-AFC model used in this study is available with instructions for download and utilisation in Supplementary Material 5 (both a blank template spreadsheet, 5a, and an example spreadsheet completed for Mt Kinabalu, 5b. Alternatively, access [URL/DOI of spreadsheet to be finalised post-acceptance] or contact the lead author for the latest version.

#### **CONCLUSIONS**

- The primary magma of Mt Kinabalu was a partial melt of fertile, metasomatised, high-K, low-Na mantle. This may have been similar to the source for the contemporaneous Linhaisai minette magmatism in central

Borneo, which would have resulted from lower degrees of melting. Magmatism was contemporaneous with and driven by regional crustal extension, possibly linked to a slab rollback during subduction of the Celebes Sea to the SE.

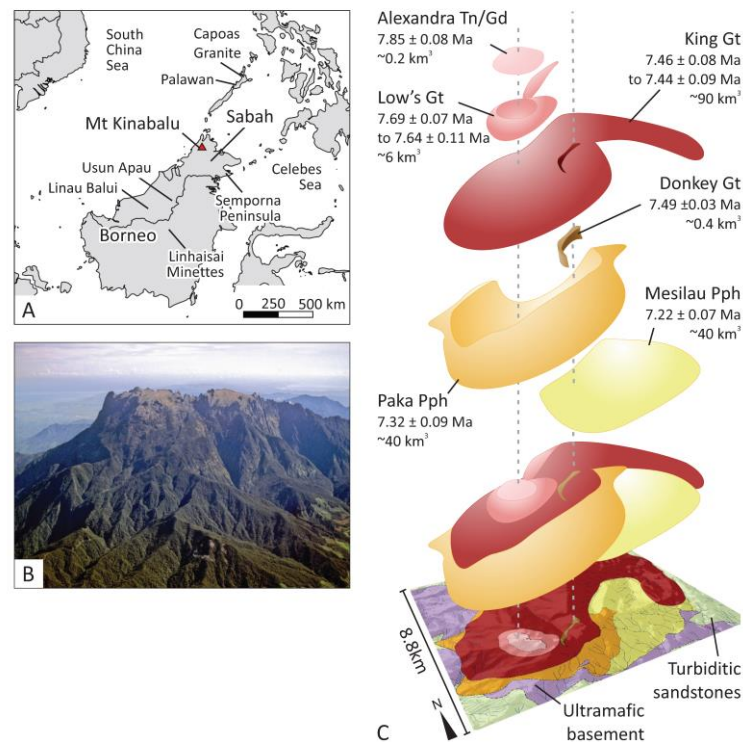
- Compiled experimental data shows that metaluminous melts with both  $\text{Ca/Na} > 1.5$  and  $\text{K/Na} > 0.5$  (Fig. 7), including Mt Kinabalu, cannot be generated through crustal anatexis.
- Fractional crystallisation of plagioclase, pyroxene, and amphibole rich cumulates from initial Mt Kinabalu magmas was accompanied by assimilation of partial melts of siliclastic sediments; most probably the basal units of the Crocker Formation. Combined with metasomatism of the mantle source, this imparted a high-K to shoshonitic chemistry to the granitoids. The fertility of the contaminating crust reduced after emplacement of the initial two granitic units, reducing the assimilation rate in subsequent magmatism. This variation in assimilation rate produced the geochemical heterogeneity of Mt Kinabalu.
- Evidence for the derivation of Mt Kinabalu granitic magmatism from assimilation and fractional crystallisation was determined through a new approach to AFC modelling of major and trace elements, and radiogenic and stable isotope ratios. The major and minor element chemistry of each fractionating phase is calculated to be in magmatic equilibrium using experimentally derived two-component partition coefficients at each stage of this incremental model (Equilibrated Major Element Assimilation and Fractional Crystallisation modelling, EME-AFC).

## ACKNOWLEDGEMENTS

We thank Wendy Bohrson, Frank Spera, Hervé Rezeau, and an anonymous reviewer for their thorough reviews of this paper, and Wendy Bohrson and Marjorie Wilson for their work as editors. We are additionally indebted to Wendy Bohrson for her discussions during revision of the manuscript. NERC supported this study through a PhD studentship to AB-J and access to the Isotope Community Support Facility at SUERC. We wish to thank Alim Biun, Felix Tongkul and Maklarin Lakim for their assistance in facilitating the field season; Jamili Nais of Sabah Parks who allowed us to work in the National Park; the mountain guides and researchers of Mt Kinabalu National Park, especially Alijen “Jen”, Halli, Jasirin, Sokaibin, Maklarin Lakim, Sapinus, Samuel and Nicholas; and we thank Robert Hall, Mike Cottam and the SE Asia Research Group at Royal Holloway for their support throughout this project.

## REFERENCES

Automatic citation updates are disabled. To see the bibliography, click Refresh in the Zotero tab.



704  
705 Fig. 1. A) Regional geography of Mt Kinabalu and the locations referred to in the text  
706 within SE Asia. B) Aerial photograph of Mt Kinabalu from the south highlighting its  
707 extreme vertical relief; courtesy of Tony Barber. C) Internal structure and U-Pb zircon  
708 emplacement ages of the Mt Kinabalu intrusion (Cottam *et al.*, 2010; Burton-  
709 Johnson *et al.*, 2017). Volumes were determined using field relations and contact  
710 orientations, as discussed in Burton-Johnson *et al.* (2017). Abbreviations: Tn –  
711 Tonalite, Gd – Granodiorite, Gt – Granite, Pph – Porphyritic Granite.

712

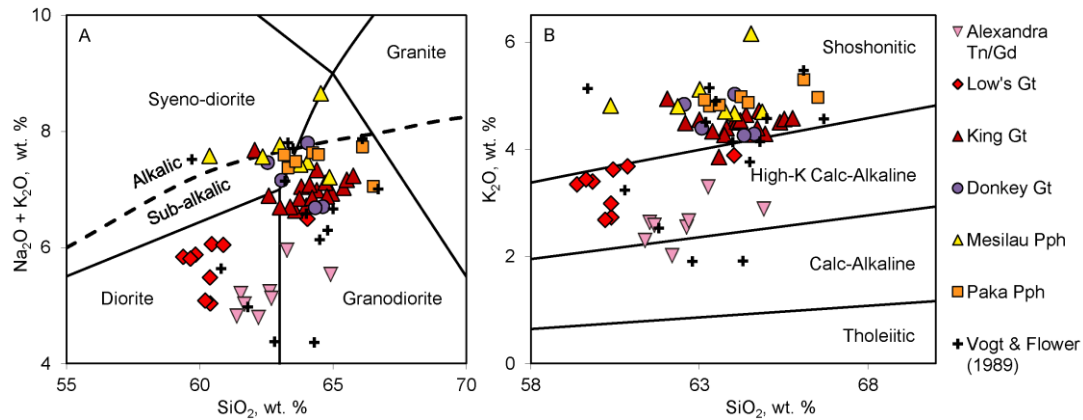


Fig. 2. Geochemical classification diagrams of the Mt Kinabalu granitoids. A) TAS diagram of Cox *et al.* (1979). B) K<sub>2</sub>O vs silica diagram of Le Maitre *et al.* (1989). Abbreviations as in Fig. 1. Existing data shown for comparison (Vogt and Flower, 1989).

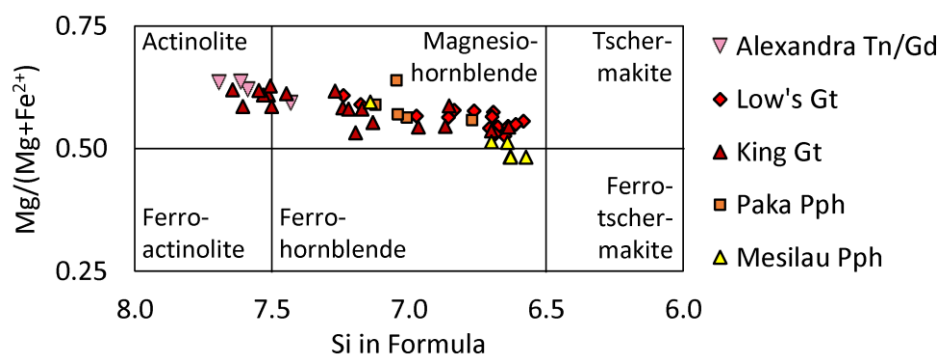


Fig. 3. Amphibole chemistries, following the Leake *et al.* (1997) classification for calcic amphiboles.



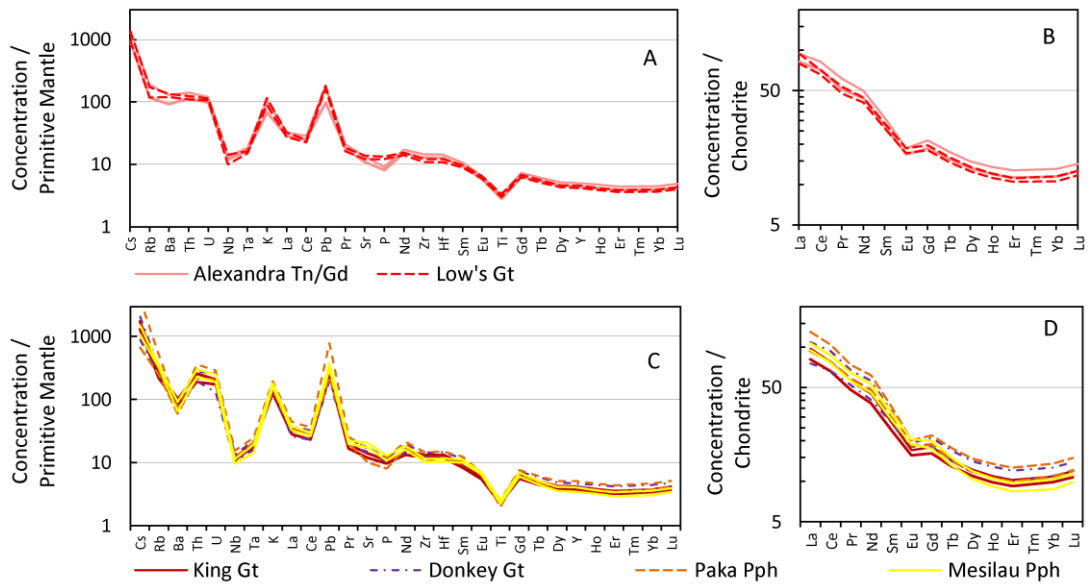


Fig. 4. Multi-element, primitive mantle normalised trace element plots and chondrite normalised REE plots for the Mt Kinabalu granitic units. Plots show the upper and lower 95% confidence limits for each unit. Normalising values from Sun and McDonough (1989). Abbreviations as in Fig. 1.

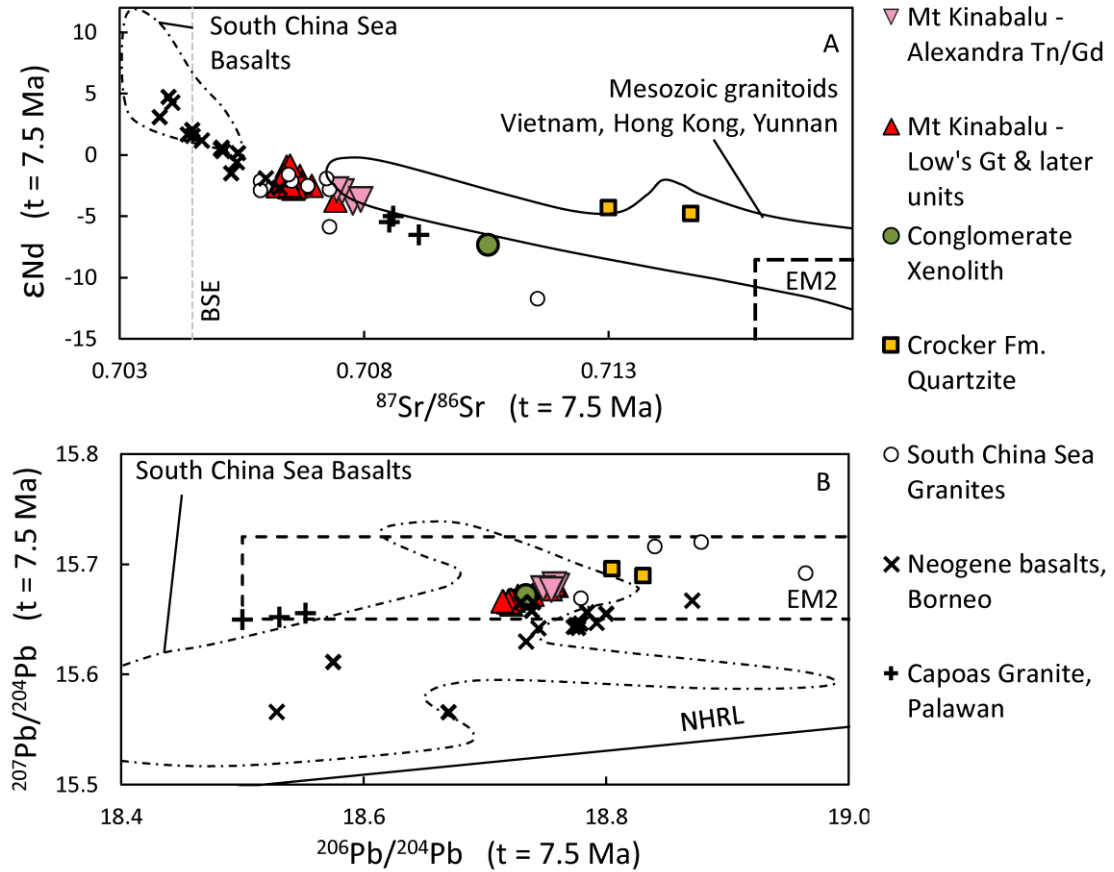


Fig. 5. Sr, Nd and Pb isotope ratios Mt Kinabalu granitic rocks at 7.5Ma. Data for comparison: South China Sea basalts (Tu *et al.*, 1992; Yan *et al.*, 2008); Mesozoic granites of the South China Block and Yangtze Block (Zhu, 1995); Mesozoic Granitoids of Vietnam (Thuy *et al.*, 2004), Hong Kong (Darbyshire and Sewell, 1997) and Yunnan Province (Yanbo and Jingwen, 2010); Neogene basalts from Borneo (Macpherson *et al.*, 2010; Cullen *et al.*, 2013); Mesozoic granites from the South China Sea (Yan *et al.*, 2010, 2011); Spreading centre basalts of the Indian Ocean from the PetDB database (<http://www.earthchem.org/petdb>); Northern Hemisphere Reference line (NHRL) backdated to 7.5Ma using the mean U & Pb concentrations of the I-MORB data (Hart, 1984). EM2 fields from Zindler and Hart (1986). Bulk Silicate Earth (BSE) from Faure (1986). Abbreviations as in Fig. 1.

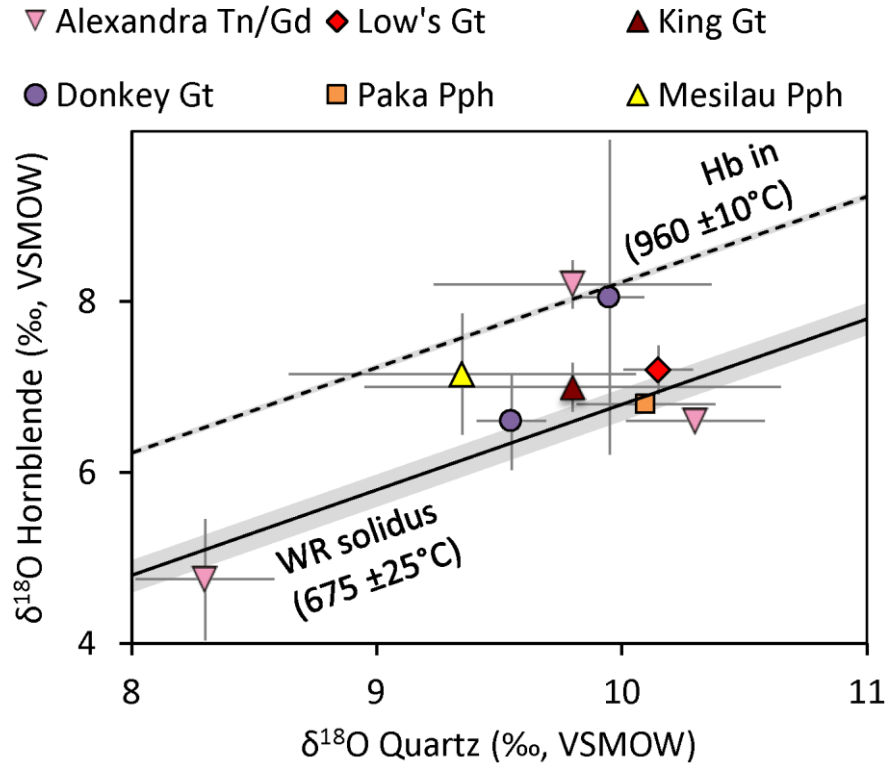
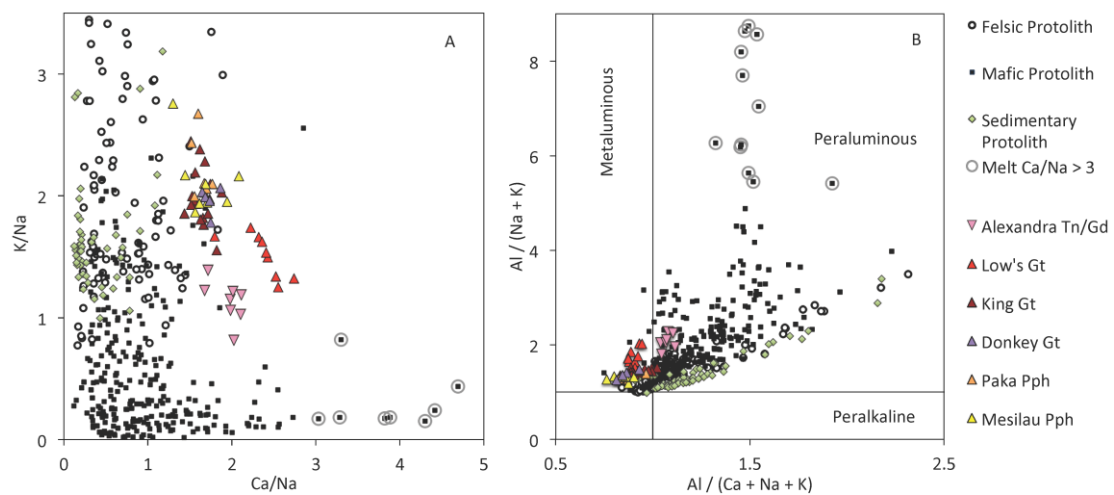


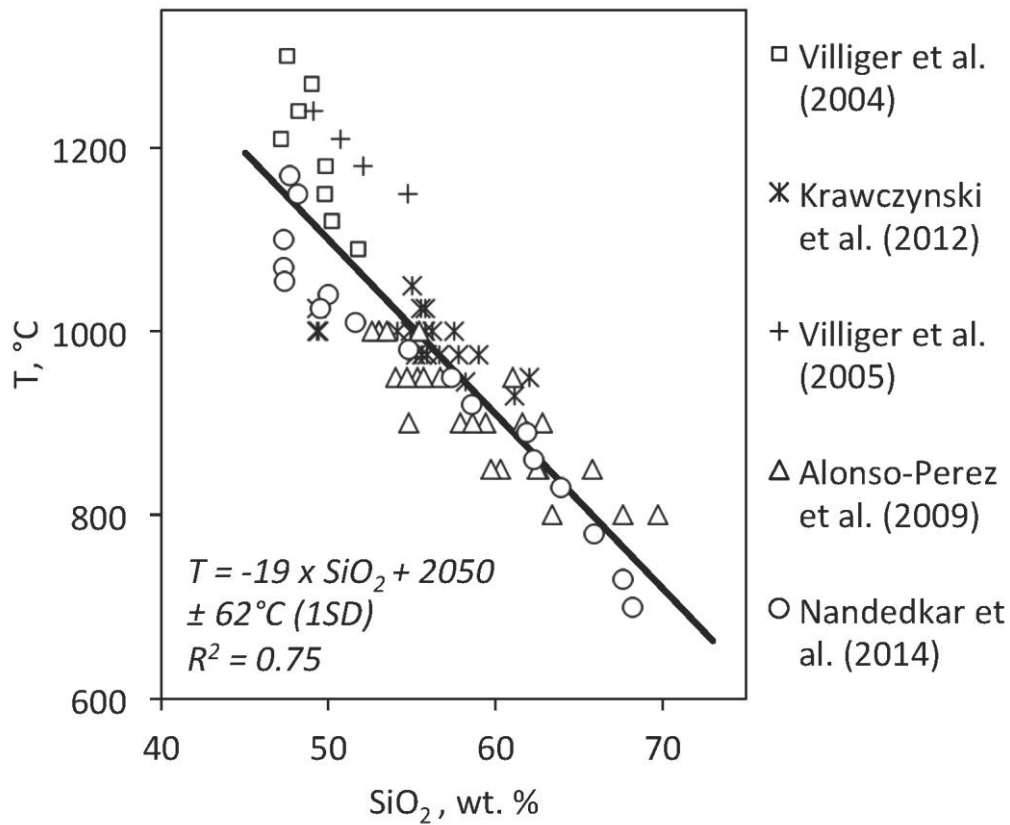
Fig. 6.  $\delta^{18}\text{O}$  values of quartz and hornblende in Mt Kinabalu rocks. 2SD error bars based on replicate analyses of each mineral from the same sample. Calculated isotherms and associated errors (grey shaded regions) shown for the whole rock solidus and hornblende crystallisation temperatures for the vapour saturated 200MPa experiments of Naney (1983) (calculated from Clayton *et al.*, 1989; Kohn and Valley, 1998; Chacko *et al.*, 2001; Valley, 2003; Lackey *et al.*, 2008). Abbreviations as in Fig. 1.



751

752 Fig. 7. Comparison of the Mt Kinabalu data with collated melting experiment data for  
 753 melting experiments on potential felsic sources (tonalites and felsic gneisses), mafic  
 754 sources (basalts and basaltic amphibolites), and sedimentary sources (sediments and  
 755 metasediments) (Vielzeuf and Holloway, 1988; Beard and Lofgren, 1991; Douce  
 756 and Johnston, 1991; Rapp *et al.*, 1991; Rushmer, 1991, 1993; Winther and  
 757 Newton, 1991; Skjerlie and Johnston, 1992; Sen and Dunn, 1994; Wolf and  
 758 Wyllie, 1994; Douce and Beard, 1995; Gardien *et al.*, 1995, 2000; Rapp and  
 759 Watson, 1995; Singh and Johannes, 1996a, 1996b; Winther, 1996; Montel and  
 760 Vielzeuf, 1997; Patino Douce, 2004; Sisson *et al.*, 2005; Xiong *et al.*, 2005; Xiao  
 761 and Clemens, 2007). Note that the samples from mafic sources showing Ca/Na  
 762 values >3 (highlighted in circles) are peraluminous with high Al/(Na+K) values.  
 763 Crustal values from Rudnick and Gao (2003). Abbreviations as in Fig. 1.

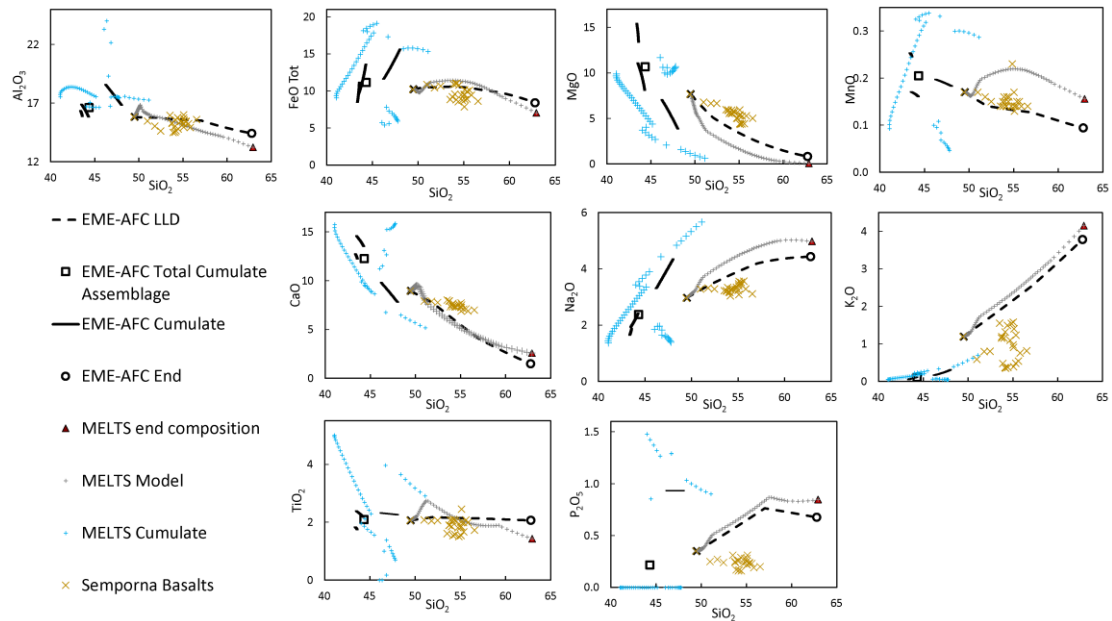
764



765

766 Fig. 8. Temperature vs  $\text{SiO}_2$  for glasses from published crystallisation experiments  
 767 and empirical relationship derived by linear regression (Villiger *et al.*, 2004; Villiger,  
 768 2005; Alonso-Perez *et al.*, 2009: 200; Krawczynski *et al.*, 2012; Nandedkar *et al.*,  
 769 2014).

770



771

772 Fig. 9. Liquid lines of descent (LLD) of major elements (wt. %) for basalt SBK13  
 773 from Semporna, northeast Borneo (Macpherson *et al.*, 2010), compared with  
 774 fractionating assemblages from Rhyolite-MELTS and EME-AFC models. Whole rock  
 775 (WR) compositions of the basaltic suite are shown for comparison (Macpherson *et al.*,  
 776 2010). Note that these are fractional crystallisation only models, and the discrepancy  
 777 between the models and sample data in the Na<sub>2</sub>O and K<sub>2</sub>O plots highlights the effect  
 778 of crustal assimilation on the differentiation of the Bornean basaltic suite  
 779 (Macpherson *et al.*, 2010).

780

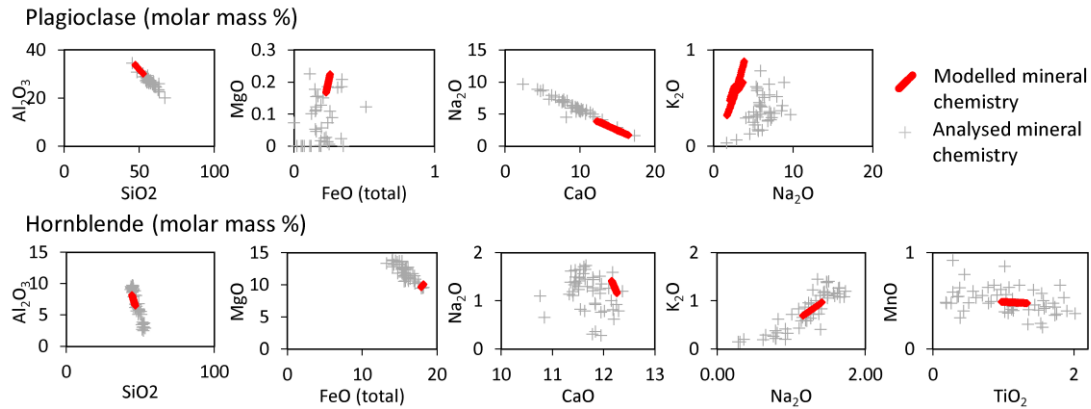


Fig. 10. Molar mass % of the analysed mineral chemistries of Mt Kinabalu and EME-AFC modelled mineral chemistries of the King Granite.

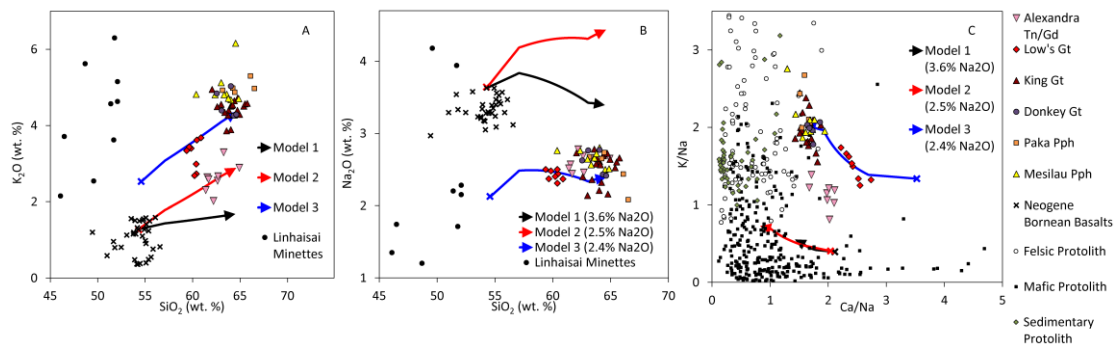
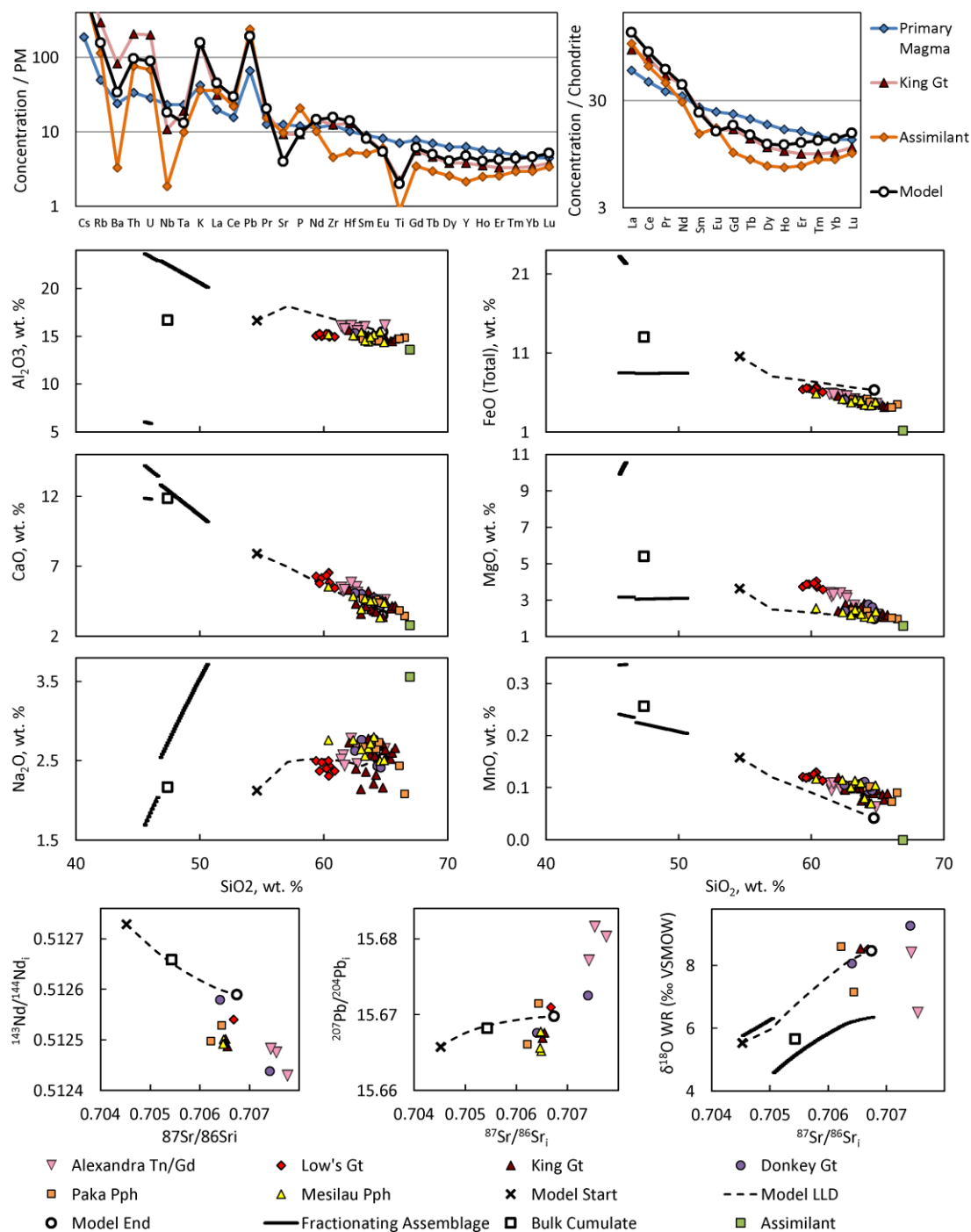


Fig. 11. Alkali metal chemistries of Mt Kinabalu granites and models to simulate assimilation with fractional crystallisation. (a)  $K_2O$  versus  $SiO_2$ , (b)  $Na_2O$  versus  $SiO_2$ , (c)  $K/Na$  versus  $Ca/Na$ . Model 1 (black): Linau Balui basalt (LB85; Cullen *et al.*, 2013) contaminated by the bulk chemistry of meta-conglomerate xenolith from the Donkey Granite. Model 2 (red): LB85 contaminated by partial melt of biotite, plagioclase and quartz-bearing starting material (BPQ) of Gardien *et al.* (1995): Model 3 (blue) Starting material with modified alkali contents as discussed in text contaminated by BPQ partial melt (as in Model 2). Experimental melt data in (c) as in Fig. 7. Neogene basalt data from Macpherson *et al.* (2010) and Cullen *et al.* (2013). Note that Model 1 is larger overlain by Model 2 in (c). Abbreviations as in Fig. 1.



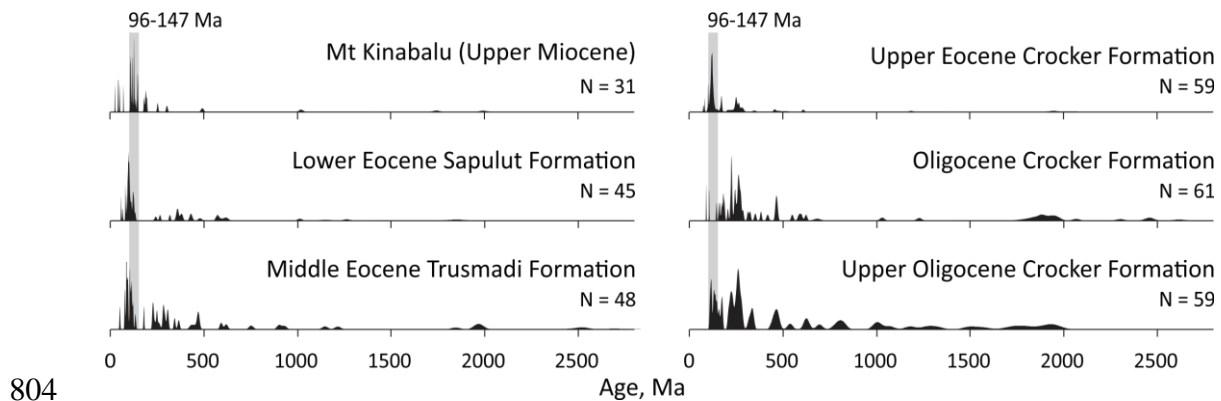
796

797 Fig. 12. Compositional comparison (isotopes, trace elements and selected major  
 798 elements) of the EME-AFC King Granite model end values, liquid line of descent  
 799 (LLD), fractionating assemblage and bulk cumulate with the primary magma (2.1%  
 800 Na<sub>2</sub>O and 2.5% K<sub>2</sub>O; Model 3 in Fig. 11), partially melted xenolith and partially  
 801 melted BPQ assimilant (used respectively for trace and major elements) and King



802 Granite target composition. Normalising values from Sun and McDonough (1989).

803 Abbreviations as in Fig. 1.



805 Fig. 13. Probability density plots of  $^{206}\text{Pb}/^{238}\text{U}$  inherited zircon ages from Mt Kinabalu  
806 (Cottam *et al.*, 2010) and  $^{206}\text{Pb}/^{238}\text{U}$  detrital zircon ages from the principal  
807 sedimentary units of Sabah: the Eocene Sapulut and Trusmadi Formations and the  
808 Eocene-Oligocene units of the Crocker Formation (van Hattum *et al.*, 2013).

809

810 Table 1. Whole rock Major and trace element data from Mt Kinabalu. \* Major  
811 element data from Sperber (2009).

812

813

814

815 Table 2. Isotopic data from Mt Kinabalu. \*Whole rock  $\delta^{18}\text{O}$  calculated from  
816 hornblende  $\delta^{18}\text{O}$  as detailed in the text.

817

818 Table 3. Two-component major element partition coefficients determined from  
819 experimental data (Grove *et al.*, 2003; Alonso-Perez *et al.*, 2009; Nandedkar *et al.*,  
820 2014), including the values used for EME-AFC modelling of Mt Kinabalu.

821

822 Table 4. Fractionating phases, parameters and outputs of the EME-AFC modelling of  
823 the compositional range of the Alexandra Tonalite/Granodiorite, the Low's Granite  
824 and the King Granite.

825

Lat.	6.0728	6.0784	6.0763	6.0756	6.0790	6.0818	6.0767	6.0712	6.1235	6.0831	6.1224	6.0310	6.0750	6.0768	6.0788
Long.	116.5570	116.5513	116.5502	116.5537	116.5500	116.5492	116.5490	116.5533	116.5720	116.5538	116.5738	116.7251	116.5587	116.5571	116.5570
Height, m	4030	3827	3929	3959	3803	3684.11	3991.24	3891.51	2586	3945	0	0	4096	3947	3847
	Alex. Gd	Alex. Gd	Alex. Gd	Alex. Gd	Alex. Gd	Alex. Gd	Alex. Gd	Alex. Gd	Low's Gt	Low's Gt	Low's Gt	Low's Gt	Low's Gt	Low's Gt	Low's Gt
	CS016	CS021	CS022	CS023	CS036	A042	A047	A054	CS077	A046	A218	SBK121	CS018	CS019	CS020
(wt%)															
SiO <sub>2</sub>	63.26	61.53	62.62	62.19	62.68	64.91	61.38	61.67	60.88	60.21	59.65	60.40	60.45	60.39	59.38
TiO <sub>2</sub>	0.65	0.68	0.66	0.72	0.66	0.54	0.63	0.66	0.63	0.66	0.68	0.71	0.67	0.69	0.67
Al <sub>2</sub> O <sub>3</sub>	15.99	15.87	15.85	16.10	15.56	16.13	16.07	15.75	14.96	15.29	15.29	15.25	14.96	15.13	15.07
FeO <sub>tot</sub>	5.14	5.84	5.42	5.70	5.53	4.54	5.81	5.79	6.07	6.19	6.56	6.74	6.44	6.56	6.43
MnO	0.10	0.10	0.10	0.10	0.10	0.06	0.11	0.11	0.11	0.13	0.12	0.13	0.12	0.13	0.12
MgO	2.72	3.23	3.24	3.39	3.10	2.23	3.40	3.32	3.59	3.94	3.87	4.05	3.72	3.83	3.74
CaO	4.73	5.28	5.54	5.84	5.14	4.61	5.49	5.35	5.47	6.36	5.80	6.57	5.87	6.55	6.30
Na <sub>2</sub> O	2.66	2.57	2.69	2.78	2.46	2.65	2.52	2.44	2.37	2.40	2.37	2.31	2.44	2.50	2.50
K <sub>2</sub> O	3.30	2.64	2.55	2.02	2.67	2.89	2.31	2.59	3.68	2.69	3.44	2.73	3.62	2.99	3.34
P <sub>2</sub> O <sub>5</sub>	0.18	0.18	0.19	0.20	0.18	0.17	0.18	0.18	0.26	0.24	0.28	0.30	0.27	0.29	0.27
Total	99.30	99.44	99.46	99.67	99.53	99.90	107.60	99.42	99.75	99.84	100.02	99.94	99.28	99.79	99.12
LOI	0.73	0.87	0.57	1.00	0.84	0.66	1.06	0.92	1.05	1.05	1.23	1.24	0.50	0.93	0.58
ppm															
Ta	0.78	0.71	0.66	0.68	0.66	0.82	0.64	0.67	0.58	0.62	0.63	0.66	0.62	0.60	0.70
Sc	14.20	22.04	17.91	21.34	21.54	12.94	20.47	20.45	21.35	21.79	22.11	17.88	17.97	18.30	17.12
V	100.34	187.45	142.53	166.38	167.06	101.80	176.00	173.00	184.49	188.30	201.10	151.50	151.41	155.76	151.54
Cr	42.20	58.87	50.84	56.45	57.66	35.12	62.96	65.45	75.68	92.40	82.55	62.35	61.20	63.80	60.12
Ga	13.97	17.75	14.50	17.62	17.67	17.68	17.94	17.71	16.65	16.93	17.67	13.74	13.81	14.17	14.05
Co	10.89	15.47	13.14	15.11	15.29	10.71	16.32	16.01	20.25	20.39	20.47	16.33	16.95	17.04	16.47
Ni	24.91	16.65	18.99	15.39	14.60	11.44	17.18	16.82	18.23	22.27	20.15	13.11	14.60	13.89	13.14
Cu	3.73	35.34	12.23	5.12	23.57	7.39	22.66	17.64	43.11	28.37	52.02	1052.8	29.28	62.40	38.56
Zn	40.50	48.60	44.49	34.90	50.79	38.10	54.04	59.54	50.76	59.52	54.50	71.75	45.11	45.67	48.48
Cs	9.17	9.45	9.41	7.71	8.25	9.57	9.71	9.00	11.32	5.46	11.75	9.12	11.57	8.93	9.73
Rb	103.26	102.26	86.82	92.40	98.63	107.30	83.80	93.55	117.35	68.08	119.50	74.43	107.97	90.63	83.41
Ba	770.96	901.42	924.83	925.12	890.96	834.60	816.00	865.50	847.28	856.00	854.30	977.93	1010.8	867.50	863.25
Sr	193.66	239.28	214.07	249.52	248.24	255.50	247.10	257.90	273.97	310.30	300.70	243.30	238.73	252.41	266.49
Zr	171.00	143.40	136.20	154.30	136.60	167.20	143.30	148.60	125.60	141.20	126.90	130.20	111.00	120.40	142.70
Hf	4.51	4.14	3.68	4.23	3.64	4.50	3.97	4.05	3.42	3.78	3.44	3.53	3.16	3.34	3.93
Th	11.58	10.09	8.86	9.87	10.22	11.53	8.92	12.42	12.17	10.20	8.98	9.58	10.01	10.14	10.00
U	2.12	2.20	1.87	2.10	1.86	2.39	2.02	2.49	2.48	2.30	2.24	2.44	2.24	2.26	2.27
Pb	11.20	7.18	8.98	4.58	7.14	10.59	9.42	9.94	12.95	13.22	12.43	12.22	11.73	11.47	13.71
Nb	10.13	8.80	8.07	8.56	8.40	10.10	8.24	8.65	7.03	7.81	14.89	7.99	7.09	7.81	8.04
Y	22.52	20.87	19.88	20.27	20.08	18.52	21.26	21.19	17.84	19.71	20.40	20.37	17.88	19.79	19.44
La	24.34	21.00	20.17	21.33	20.53	21.73	19.17	19.94	17.32	18.41	22.52	19.26	19.90	20.12	19.73
Ce	53.38	49.06	40.01	44.14	42.32	53.30	42.83	45.92	37.70	43.87	40.88	40.60	39.31	41.47	44.03
Pr	5.97	5.52	4.16	4.60	4.39	5.82	5.27	5.10	4.03	4.82	5.12	4.67	4.19	4.80	4.87
Nd	24.07	22.08	19.01	20.75	19.73	23.51	19.03	21.24	18.46	20.01	17.74	19.63	19.01	20.40	20.63
Sm	4.59	4.36	3.91	4.14	4.01	4.44	4.28	4.20	3.76	4.07	4.23	4.09	3.87	4.18	4.22
Eu	0.98	1.01	0.96	0.97	0.93	0.99	1.03	1.03	0.98	0.99	1.13	1.01	0.97	1.00	1.03
Gd	4.20	4.11	3.63	3.86	3.74	3.67	4.17	3.88	3.50	3.73	4.04	3.84	3.62	3.82	3.93
Tb	0.60	0.62	0.56	0.60	0.59	0.55	0.61	0.60	0.53	0.56	0.60	0.55	0.54	0.58	0.57
Dy	3.55	3.60	3.29	3.47	3.35	3.09	3.60	3.52	3.10	3.24	3.31	3.23	3.15	3.28	3.28
Ho	0.73	0.74	0.67	0.71	0.67	0.62	0.75	0.71	0.61	0.64	0.65	0.66	0.62	0.66	0.66
Er	1.96	1.94	1.85	1.94	1.83	1.67	2.05	1.95	1.67	1.78	1.76	1.78	1.70	1.80	1.79
Tm	0.28	0.28	0.31	0.34	0.31	0.26	0.24	0.31	0.29	0.27	0.13	0.25	0.29	0.27	0.27
Yb	2.12	2.09	1.92	2.00	1.91	1.75	2.14	2.05	1.70	1.83	1.91	1.93	1.74	1.84	1.82
Lu	0.34	0.36	0.31	0.32	0.32	0.28	0.35	0.34	0.29	0.30	0.31	0.33	0.29	0.30	0.31

826

827 Table 1. Whole rock Major and trace element data from Mt Kinabalu. \*Major element

828 data from Sperber (2009).

829

Lat.	6.1214	6.0733	6.0640	6.0640	6.0766	6.0788	6.0943	6.0741	6.0589	6.0729	6.0705	6.0684	6.0740	6.0738	6.0791	6.0800
Long.	116.5776	116.5575	116.5670	116.5704	116.5758	116.5810	116.5807	116.5790	116.5653	116.5704	116.5703	116.5704	116.6282	116.6168	116.5259	116.5298
Height, m	3025	0	3577	3460	3918	3769	3657	4007	3241.9	3488.96	3611.29	3767.98	3007.82	3126.3	1886.21	2150.33
	Low's Gt	King Gt	King Gt	King Gt	King Gt	King Gt	King Gt	King Gt	King Gt	King Gt	King Gt	King Gt	King Gt	King Gt	King Gt	King Gt
	CS081	SBK123	CS011 c	CS028	CS031	CS066	CS069	CS072	A089c	A128	A129	A131	A236	A237	A282	A285
(wt%)																
SiO <sub>2</sub>	59.84	64.04	64.40	64.39	63.59	62.06	64.01	64.96	64.12	64.72	65.53	65.77	63.39	63.01	64.77	62.59
TiO <sub>2</sub>	0.67	0.53	0.52	0.52	0.52	0.53	0.55	0.47	0.50	0.47	0.41	0.44	0.51	0.52	0.48	0.54
Al <sub>2</sub> O <sub>3</sub>	15.02	14.81	14.53	15.13	15.12	15.63	15.30	14.84	14.70	14.88	14.48	14.74	15.06	15.34	14.97	15.06
FeO <sub>TOT</sub>	6.52	5.04	4.35	4.68	4.89	5.57	5.22	4.64	4.94	4.74	4.14	4.27	5.10	5.10	4.75	5.34
MnO	0.12	0.09	0.07	0.09	0.10	0.12	0.11	0.10	0.09	0.09	0.08	0.09	0.10	0.10	0.10	0.10
MgO	3.87	2.81	2.74	2.60	2.32	2.41	2.82	2.39	2.54	2.40	2.08	2.19	2.64	2.64	2.41	2.78
CaO	6.20	4.86	4.68	4.39	5.25	5.32	3.85	4.53	4.61	4.60	4.18	4.18	4.15	3.60	3.39	4.34
Na <sub>2</sub> O	2.48	2.61	2.71	2.69	2.78	2.73	2.21	2.64	2.56	2.72	2.60	2.66	2.36	2.14	2.16	2.40
K <sub>2</sub> O	3.40	3.89	4.28	4.65	3.86	4.95	4.51	4.29	4.52	4.40	4.57	4.58	4.34	4.56	4.73	4.50
P <sub>2</sub> O <sub>5</sub>	0.28	0.20	0.23	0.24	0.26	0.29	0.23	0.21	0.22	0.21	0.18	0.18	0.23	0.24	0.20	0.24
Total	99.75	99.96	99.64	99.90	99.24	100.23	99.39	100.09	99.90	100.32	99.32	100.05	100.02	100.15	100.30	100.03
LOI	0.61	0.52	0.64	1.11	0.77	0.36	1.87	0.49	0.54	0.56	0.60	0.47	1.57	2.33	1.81	1.55
ppm																
Ta	0.70	0.78	0.96	0.82	0.96	0.75	0.81	0.81	0.75	0.64	0.69	0.82	0.73	0.75	0.78	0.68
Sc	25.38	16.83	17.04	13.84	14.24	14.64	15.98	15.56	15.81	14.28	12.29	12.75	15.73	16.03	14.67	17.29
V	211.19	141.75	145.30	115.51	128.08	132.57	112.15	128.95	134.80	123.80	110.70	111.30	134.50	132.90	125.40	147.00
Cr	86.95	58.35	53.81	39.79	31.06	26.75	81.18	46.97	45.75	41.78	37.58	38.94	47.08	47.23	43.60	51.33
Ga	17.65	15.71	16.45	12.25	13.66	13.95	11.85	15.66	16.09	15.76	15.33	15.49	16.10	15.91	16.15	16.56
Co	23.59	15.37	12.67	12.58	10.94	12.59	13.63	14.30	13.29	14.05	12.07	12.74	14.72	15.20	13.62	15.01
Ni	21.19	14.41	12.77	8.78	5.70	4.66	42.73	12.31	12.27	11.72	10.25	11.86	12.83	12.77	11.87	13.62
Cu	59.84	41.01	30.50	21.90	5.70	40.82	8.18	33.83	56.78	26.90	22.19	9.50	18.93	14.43	11.64	16.00
Zn	58.31	41.66	43.02	44.54	30.50	34.30	80.77	44.58	43.56	39.86	32.78	40.89	48.25	49.98	44.44	43.56
Cs	10.08	17.65	12.97	15.04	5.56	9.66	10.34	13.63	18.75	8.65	9.55	17.32	8.88	10.45	13.48	9.93
Rb	119.46	140.99	165.50	166.03	97.37	153.96	144.18	160.97	188.70	158.30	174.60	197.10	155.20	173.70	187.40	167.30
Ba	912.61	883.93	605.60	865.41	677.98	586.81	825.67	661.57	650.50	680.00	623.10	644.00	653.50	720.80	576.50	700.20
Sr	314.28	261.09	283.90	181.39	295.92	293.62	164.05	283.56	296.70	314.10	293.20	288.70	256.80	232.80	195.70	271.00
Zr	140.00	132.80	149.80	132.70	155.10	205.90	137.50	120.10	127.60	135.70	126.70	128.60	140.30	136.10	140.10	142.20
Hf	3.92	3.65	4.28	3.77	4.38	5.63	3.84	3.33	3.45	3.63	3.42	3.68	3.81	3.83	4.03	3.91
Th	10.14	17.71	23.69	13.14	26.48	19.45	14.86	15.58	42.61	21.66	15.98	18.84	18.69	17.14	17.57	9.04
U	2.44	3.83	5.20	3.17	5.18	4.99	3.30	3.57	5.14	4.47	3.87	5.19	3.78	3.50	4.23	2.74
Pb	12.79	13.04	18.06	25.07	13.03	21.02	23.53	19.13	21.76	16.64	16.14	20.48	18.89	20.58	16.74	17.85
Nb	8.01	7.64	8.71	8.76	9.99	8.31	8.79	7.89	8.01	7.17	6.77	7.54	7.86	8.06	7.73	7.57
Y	19.82	15.39	19.69	18.72	23.68	19.73	20.74	15.90	17.37	16.30	15.03	14.99	18.18	18.35	17.36	18.14
La	26.52	16.58	19.70	23.10	39.21	23.75	22.24	20.21	18.95	19.85	17.88	21.09	19.84	23.63	21.35	17.06
Ce	44.20	37.63	50.81	42.66	73.18	51.13	47.99	37.50	37.62	38.99	34.07	38.23	43.21	49.15	45.40	40.82
Pr	5.11	4.07	5.51	4.41	7.69	5.91	5.54	3.88	4.67	4.42	4.05	4.51	4.85	5.21	4.91	4.72
Nd	20.81	16.15	22.13	20.19	30.22	23.75	22.37	17.11	16.30	18.30	13.79	14.96	20.19	21.50	19.84	19.69
Sm	4.22	3.15	4.38	4.11	5.63	4.90	4.49	3.39	3.79	3.66	3.22	3.38	4.03	4.13	3.80	3.98
Eu	1.03	0.78	1.07	0.90	1.16	1.13	0.98	0.87	0.96	0.91	0.87	0.88	0.97	1.00	0.92	0.97
Gd	3.88	2.84	3.88	3.58	4.66	4.25	3.97	2.98	3.42	3.18	2.83	3.10	3.40	3.62	3.33	3.56
Tb	0.57	0.40	0.60	0.55	0.71	0.60	0.57	0.45	0.49	0.48	0.41	0.44	0.51	0.54	0.50	0.52
Dy	3.34	2.45	3.28	3.15	3.90	3.44	3.34	2.57	2.87	2.70	2.37	2.58	2.97	3.08	2.79	3.01
Ho	0.67	0.48	0.67	0.61	0.78	0.68	0.68	0.52	0.56	0.54	0.48	0.51	0.60	0.62	0.58	0.61
Er	1.78	1.29	1.84	1.73	2.13	1.85	1.80	1.43	1.56	1.49	1.30	1.36	1.65	1.73	1.58	1.61
Tm	0.24	0.19	0.29	0.29	0.34	0.27	0.25	0.24	0.16	0.24	0.11	0.12	0.26	0.27	0.25	0.26
Yb	1.94	1.47	1.95	1.85	2.26	2.11	1.96	1.54	1.67	1.63	1.48	1.55	1.74	1.83	1.68	1.76
Lu	0.32	0.25	0.33	0.30	0.36	0.37	0.33	0.26	0.27	0.26	0.24	0.25	0.28	0.30	0.28	0.29

830

831 Table 1. (cont.)

Lat.	6.0798	6.0880	6.0705	6.0747	6.0819	6.0665	6.0565	6.0514	6.0555	6.0638	6.0734	6.0747	6.0819	6.0665	6.0565
Long.	116.5350	116.5780	116.5647	116.5697	116.5780	116.5640	116.5646	116.5639	116.5647	116.5739	116.5844	116.5697	116.5780	116.5640	116.5646
Height, m	2443.77	3767	3946.06	3389.22	3805.71	3755.96	0	0	3096	3508.18	3888.38	3389.22	3805.71	3755.96	0
	King Gt	Donkey Gt	Donkey Gt	Donkey Gt	Donkey Gt	Donkey Gt	Paka Pph	Paka Pph	Paka Pph	Paka Pph	Paka Pph	Donkey Gt	Donkey Gt	Donkey Gt	Paka Pph
	A286	CS033	A093	A127	A145	A079	SBK128	SBK130	CS027	A155	A162	A127	A145	A079	SBK128
(wt%)															
SiO <sub>2</sub>	64.22	64.06	64.63	63.08	62.56	64.34	64.25	66.53	66.11	64.46	63.17	63.08	62.56	64.34	64.25
TiO <sub>2</sub>	0.49	0.48	0.54	0.49	0.52	0.57	0.52	0.45	0.45	0.47	0.50	0.49	0.52	0.57	0.52
Al <sub>2</sub> O <sub>3</sub>	15.10	14.76	14.70	15.16	15.32	14.89	14.55	14.84	14.71	14.49	14.70	15.16	15.32	14.89	14.55
FeO <sub>TOT</sub>	4.78	5.04	4.72	4.95	5.03	4.85	5.14	4.48	4.08	4.76	5.09	4.95	5.03	4.85	5.14
MnO	0.10	0.11	0.09	0.10	0.10	0.09	0.10	0.09	0.07	0.10	0.10	0.10	0.10	0.09	0.10
MgO	2.47	2.17	2.60	2.30	2.41	2.75	2.40	1.96	2.02	2.13	2.44	2.30	2.41	2.75	2.40
CaO	3.76	4.73	4.21	5.01	5.08	4.38	4.60	3.45	3.84	4.41	4.70	5.01	5.08	4.38	4.60
Na <sub>2</sub> O	2.32	2.77	2.41	2.76	2.62	2.43	2.65	2.08	2.43	2.73	2.67	2.76	2.62	2.43	2.65
K <sub>2</sub> O	4.54	5.03	4.29	4.39	4.84	4.26	4.98	4.97	5.30	4.87	4.92	4.39	4.84	4.26	4.98
P <sub>2</sub> O <sub>5</sub>	0.21	0.25	0.22	0.24	0.25	0.23	0.27	0.22	0.22	0.24	0.25	0.24	0.25	0.23	0.27
Total	100.10	100.25	99.71	99.36	99.80	99.93	100.03	99.57	100.07	99.56	99.59	99.36	99.80	99.93	100.03
LOI	1.59	0.29	0.76	0.33	0.51	0.59	0.20	1.38	0.38	0.38	0.47	0.33	0.51	0.59	0.20
ppm															
Ta	0.68	0.92	0.83	0.62	0.75	0.83	1.01	1.11	0.90	0.82	0.88	0.62	0.75	0.83	1.01
Sc	15.47	15.30	16.01	14.74	15.22	16.11	11.49	9.98	12.89	13.89	15.35	14.74	15.22	16.11	11.49
V	125.80	139.25	117.00	139.30	144.40	119.10	109.92	95.34	122.22	138.00	152.50	139.30	144.40	119.10	109.92
Cr	44.68	27.98	47.09	35.63	35.96	50.97	24.65	22.29	31.93	32.81	43.18	35.63	35.96	50.97	24.65
Ga	15.92	15.96	16.57	16.61	17.40	16.77	13.15	13.15	14.79	15.77	16.46	16.61	17.40	16.77	13.15
Co	14.33	14.41	12.50	14.04	14.02	12.68	9.20	9.55	14.23	13.87	15.40	14.04	14.02	12.68	9.20
Ni	11.87	7.88	11.29	10.00	10.09	12.36	6.99	5.18	9.78	9.73	12.53	10.00	10.09	12.36	6.99
Cu	14.52	23.21	16.69	26.39	31.78	26.31	105.34	47.95	143.70	35.64	44.41	26.39	31.78	26.31	105.34
Zn	42.65	44.63	59.55	40.96	32.48	58.49	26.23	30.63	31.11	39.30	36.46	40.96	32.48	58.49	26.23
Cs	12.66	12.25	17.95	8.15	7.87	13.81	7.90	11.14	10.74	16.77	12.16	8.15	7.87	13.81	7.90
Rb	189.50	202.78	178.60	150.80	182.00	177.10	175.83	170.41	233.82	224.00	221.80	150.80	182.00	177.10	175.83
Ba	679.00	567.97	561.90	646.80	675.60	591.90	511.13	469.77	441.85	463.70	579.50	646.80	675.60	591.90	511.13
Sr	244.30	328.89	302.80	360.20	361.20	322.80	270.88	209.50	300.51	344.00	377.30	360.20	361.20	322.80	270.88
Zr	130.40	134.70	161.60	138.90	154.30	179.90	124.30	130.90	117.80	118.60	135.90	138.90	154.30	179.90	124.30
Hf	3.67	4.07	4.62	3.80	4.19	4.77	3.89	4.09	3.52	3.43	4.05	3.80	4.19	4.77	3.89
Th	16.97	24.40	20.90	17.42	17.01	14.69	27.64	30.93	28.21	10.54	26.72	17.42	17.01	14.69	27.64
U	4.00	6.14	4.10	3.66	2.73	3.14	6.46	5.80	4.82	3.94	6.30	3.66	2.73	3.14	6.46
Pb	16.41	20.45	24.38	16.22	13.65	21.75	25.55	23.71	17.83	19.31	22.55	16.22	13.65	21.75	25.55
Nb	7.57	8.80	9.76	7.49	7.59	10.29	9.00	9.74	8.19	8.33	8.85	7.49	7.59	10.29	9.00
Y	16.82	20.18	21.73	20.01	19.24	22.27	18.11	22.11	18.19	18.70	18.91	20.01	19.24	22.27	18.11
La	20.48	22.70	26.84	17.73	19.40	24.07	19.98	30.43	28.31	17.42	24.71	17.73	19.40	24.07	19.98
Ce	46.25	47.97	60.79	44.21	41.95	54.53	48.93	57.24	54.11	36.46	55.81	44.21	41.95	54.53	48.93
Pr	4.87	5.62	6.67	5.08	5.17	6.63	5.85	6.70	5.55	4.81	6.23	5.08	5.17	6.63	5.85
Nd	19.83	22.74	27.12	22.00	18.05	23.68	24.13	26.84	24.28	17.98	25.34	22.00	18.05	23.68	24.13
Sm	3.82	4.60	5.24	4.38	4.21	5.22	4.97	5.14	4.45	4.37	4.97	4.38	4.21	5.22	4.97
Eu	0.93	1.03	1.13	1.09	1.08	1.21	1.13	1.16	1.00	1.07	1.13	1.09	1.08	1.21	1.13
Gd	0.30	3.94	4.45	3.84	3.83	4.63	4.16	4.21	3.67	3.94	4.00	3.84	3.83	4.63	4.16
Tb	0.49	0.55	0.66	0.57	0.55	0.66	0.56	0.60	0.52	0.51	0.56	0.57	0.55	0.66	0.56
Dy	2.77	3.04	3.73	3.23	3.12	3.77	3.13	3.37	2.90	3.00	3.14	3.23	3.12	3.77	3.13
Ho	0.56	0.62	0.76	0.67	0.62	0.75	0.63	0.68	0.59	0.59	0.63	0.67	0.62	0.75	0.63
Er	1.54	1.74	2.08	1.80	1.67	2.14	1.69	1.87	1.66	1.62	1.71	1.80	1.67	2.14	1.69
Tm	0.25	0.25	0.32	0.29	0.16	0.24	0.25	0.27	0.29	0.14	0.28	0.29	0.16	0.24	0.25
Yb	1.65	2.05	2.20	1.88	1.90	2.26	1.93	2.19	1.83	1.82	1.90	1.88	1.90	2.26	1.93
Lu	0.27	0.34	0.36	0.31	0.30	0.36	0.33	0.37	0.31	0.29	0.30	0.31	0.30	0.36	0.33

832

833 Table 1. (cont.)

Lat.	6.0514	6.0555	6.0638	6.0734	6.0665	6.0814	6.0793	6.0800	6.0723	6.0494	6.0733	6.0595	6.0595	6.132023	6.03124	6.070546
Long.	116.5639	116.5647	116.5739	116.5844	116.5815	116.5867	116.5909	116.5999	116.6012	116.5891	116.6143	116.5936	116.5940	116.5698	116.5483	116.5642
Height, m	0	3096	3508.18	3888.38	3769	3332	3513	3133	3413	2715	3134	2393	2393	2239	1874	3968
	Paka Pph	Paka Pph	Paka Pph	Paka Pph	Mes Pph	Mes Pph	Mes Pph	Mes Pph	Mes Pph	Mes Pph	Mes Pph	Mes Pph	Mes Pph	Quartzite	Sst	Xenolith
	SBK130	CS027	A155	A162	A152	A167	A170	A172	A173	A190	A241	CS055	CS056	A221	A291	A098
(wt%)																
SiO <sub>2</sub>	66.53	66.11	64.46	63.17	63.61	64.87	63.32	62.37	63.01	60.38	63.77	64.04	64.54	77.95	83.81	83.42
TiO <sub>2</sub>	0.45	0.45	0.47	0.50	0.51	0.48	0.52	0.52	0.47	0.53	0.49	0.48	0.50	0.51	0.46	0.20
Al <sub>2</sub> O <sub>3</sub>	14.84	14.71	14.49	14.70	14.45	14.36	14.55	15.10	15.43	15.18	14.91	15.19	15.52	10.62	8.40	8.08
FeO <sub>TOT</sub>	4.48	4.08	4.76	5.09	5.12	4.80	5.16	5.18	4.72	5.87	5.01	4.40	4.37	4.15	1.75	1.26
MnO	0.09	0.07	0.10	0.10	0.11	0.11	0.11	0.11	0.10	0.12	0.11	0.08	0.07	0.05	0.01	0.01
MgO	1.96	2.02	2.13	2.44	2.41	2.38	2.48	2.35	2.19	2.58	2.24	2.10	2.03	1.59	0.64	0.99
CaO	3.45	3.84	4.41	4.70	4.60	4.40	4.70	4.88	3.96	5.58	4.56	4.54	3.37	0.03	-0.05	1.90
Na <sub>2</sub> O	2.08	2.43	2.73	2.67	2.66	2.51	2.56	2.76	2.64	2.76	2.72	2.80	2.50	0.21	1.79	1.37
K <sub>2</sub> O	4.97	5.30	4.87	4.92	4.82	4.70	4.81	4.80	5.13	4.82	4.71	4.67	6.16	2.03	1.03	1.49
P <sub>2</sub> O <sub>5</sub>	0.22	0.22	0.24	0.25	0.25	0.23	0.25	0.26	0.23	0.31	0.24	0.22	0.24	0.06	0.07	0.04
Total	99.57	100.07	99.56	99.59	99.49	100.06	99.55	99.41	99.43	99.21	99.96	100.08	99.79	99.87	99.70	99.88
LOI	1.38	0.38	0.38	0.47	0.38	0.69	0.50	0.50	1.02	0.43	0.64	1.06	1.68	2.21	1.60	
ppm																
Ta	1.11	0.90	0.82	0.88	1.00	0.81	0.76	0.77	0.59	0.45	0.80	0.59	0.61	0.75	0.56	0.31
Sc	9.98	12.89	13.89	15.35	15.17	14.47	15.93	14.90	14.12	16.24	14.88	14.02	10.44	8.39	4.94	3.77
V	95.34	122.22	138.00	152.50	146.10	139.40	153.50	151.30	134.20	177.70	145.70	135.70	92.37	67.99	49.69	29.08
Cr	22.29	31.93	32.81	43.18	41.46	44.92	49.28	37.89	39.13	28.72	35.15	36.54	20.51	51.51	29.31	25.95
Ga	13.15	14.79	15.77	16.46	16.72	15.97	16.07	17.40	16.70	17.01	16.87	16.62	13.17	11.48	8.32	8.00
Co	9.55	14.23	13.87	15.40	15.38	14.46	15.63	15.27	13.94	17.80	14.80	14.21	8.93	7.79	2.04	4.82
Ni	5.18	9.78	9.73	12.53	12.38	11.87	13.34	11.06	11.20	9.39	10.52	10.00	2.43	21.91	7.25	34.96
Cu	47.95	143.70	35.64	44.41	51.80	206.10	1.96	57.62	81.57	54.91	53.99	262.78	347.06	19.44	7.20	6.37
Zn	30.63	31.11	39.30	36.46	46.21	42.32	44.33	49.67	50.75	49.10	52.40	35.21	19.91	44.64	32.70	10.61
Cs	11.14	10.74	16.77	12.16	12.99	12.39	9.55	12.42	10.94	8.89	13.41	7.34	8.36	6.79	3.77	9.03
Rb	170.41	233.82	224.00	221.80	225.00	203.00	216.60	209.60	216.90	182.20	219.70	238.44	221.90	96.26	46.23	111.50
Ba	469.77	441.85	463.70	579.50	446.30	368.30	460.90	560.10	610.70	729.00	446.10	379.01	450.60	201.90	141.20	137.40
Sr	209.50	300.51	344.00	377.30	343.20	335.40	365.50	425.20	410.10	438.30	386.30	419.03	334.79	38.71	35.01	133.90
Zr	130.90	117.80	118.60	135.90	114.60	133.70	120.50	135.70	117.20	134.50	118.40	107.00	99.45	230.80	274.80	24.11
Hf	4.09	3.52	3.43	4.05	3.34	3.76	3.42	3.86	3.28	3.48	3.50	3.03	2.83	6.08	7.13	0.67
Th	30.93	28.21	10.54	26.72	19.12	15.11	28.49	25.16	21.88	22.20	28.05	26.15	26.17	9.16	8.74	5.12
U	5.80	4.82	3.94	6.30	6.48	3.92	5.01	4.53	4.41	3.61	5.72	5.20	4.95	2.08	2.01	1.15
Pb	23.71	17.83	19.31	22.55	24.41	20.32	23.42	23.94	26.45	20.60	25.46	19.64	22.82	6.23	7.96	7.59
Nb	9.74	8.19	8.33	8.85	9.32	8.02	7.94	8.65	7.04	5.82	8.38	6.75	6.69	8.85	6.47	3.25
Y	22.11	18.19	18.70	18.91	20.02	17.93	16.92	19.62	16.67	13.81	19.24	14.53	13.87	19.29	20.23	10.26
La	30.43	28.31	17.42	24.71	21.62	25.69	24.77	25.95	25.01	20.53	27.37	20.97	26.07	20.54	22.52	14.53
Ce	57.24	54.11	36.46	55.81	46.64	49.55	51.36	57.97	51.57	40.90	58.16	47.20	46.94	42.96	39.21	27.94
Pr	6.70	5.55	4.81	6.23	5.92	5.99	5.69	6.54	5.76	4.48	6.59	5.04	4.96	5.27	5.48	3.43
Nd	26.84	24.28	17.98	25.34	21.11	21.10	23.72	27.44	23.72	18.91	27.50	22.24	22.09	19.69	21.09	12.53
Sm	5.14	4.45	4.37	4.97	4.83	4.75	4.66	5.35	4.65	3.72	5.30	4.38	4.07	3.87	4.37	2.31
Eu	1.16	1.00	1.07	1.13	1.11	1.08	1.08	1.19	1.17	1.08	1.17	1.08	1.07	0.60	0.92	0.67
Gd	4.21	3.67	3.94	4.00	4.31	4.31	3.74	4.19	3.69	3.07	4.14	3.44	3.15	3.57	4.39	2.02
Tb	0.60	0.52	0.51	0.56	0.57	0.56	0.52	0.59	0.52	0.43	0.57	0.46	0.44	0.58	0.64	0.31
Dy	3.37	2.90	3.00	3.14	3.12	3.06	2.86	3.18	2.81	2.31	3.20	2.53	2.36	3.32	3.42	1.71
Ho	0.68	0.59	0.59	0.63	0.62	0.59	0.57	0.62	0.57	0.45	0.64	0.51	0.46	0.70	0.70	0.33
Er	1.87	1.66	1.62	1.71	1.69	1.59	1.53	1.71	1.53	1.21	1.71	1.33	1.27	1.96	1.90	0.89
Tm	0.27	0.29	0.14	0.28	0.15	0.14	0.24	0.28	0.24	0.19	0.27	0.23	0.22	0.32	0.30	0.14
Yb	2.19	1.83	1.82	1.90	1.91	1.81	1.60	1.88	1.63	1.26	1.84	1.44	1.33	2.07	1.94	0.84
Lu	0.37	0.31	0.29	0.30	0.31	0.30	0.27	0.31	0.28	0.22	0.30	0.24	0.23	0.35	0.33	0.13

834

835 Table 1. (cont.)

836

Lithology	Sample	$\delta^{18}\text{O}_{\text{V-SMOW}} (\text{‰})$																Whole $\delta^{18}\text{O} (\text{‰})^*$	Rock
		$^{87}\text{Sr}/^{86}\text{Sr}_{\text{m}}$	2SE	$^{143}\text{Nd}/^{144}\text{Nd}_{\text{m}}$	2SE	$^{206}\text{Pb}/^{204}\text{Pb}_{\text{m}}$	2SE	$^{207}\text{Pb}/^{204}\text{Pb}_{\text{m}}$	2SE	$^{208}\text{Pb}/^{204}\text{Pb}_{\text{m}}$	2SE	Hornblende	SD	Quartz	SD	Biotite	SD		
Alexandra Tn/Gd	A042	0.707888	11	0.512435	08	18.7761	06	15.6811	07	39.0200	34								
Alexandra Tn/Gd	A047	0.707640	10	0.512482	07	18.7729	11	15.6823	10	39.0192	43	4.8	0.4	8.3	0.1	-1.3	0.4		6.9
Alexandra Tn/Gd	A049	0.707939	07	0.512449	11	18.7763	06	15.6791	07	39.0151	31	8.2	0.14	9.8	0.3				9.1
Alexandra Tn/Gd	A054	0.707536	18	0.512488	04	18.7732	12	15.6780	12	39.0094	31	6.6	0.0	10.3	0.1	4.9	0.3		8.4
Low's Gt	A046											7.0	0.4						8.3
Low's Gt	A218	0.706805	18	0.512548	06	18.7477	09	15.6716	09	38.9647	30	7.2	0.1	10.2	0.1	5.9	0.4		8.5
Low's Gt	SBK122	0.706989	09	0.512505	08	18.7463	06	15.6698	08	38.9574	34								
King Gt	A236	0.706702	12	0.512508	08	18.7387	08	15.6676	08	38.9488	47								
King Gt	A282	0.706849	08	0.512493	10	18.7397	08	15.6685	07	38.9460	27	7.0	0.1	9.8	0.4	0.3	0.3		8.5
Donkey Gt	A093	0.707595	16	0.512443	09	18.7518	12	15.6731	12	38.9766	41	8.1	0.9	10.0	0.1				9.3
Donkey Gt	A096											7.5	0.1						9.0
Donkey Gt	A127	0.706542	17	0.512584	04	18.7366	10	15.6683	09	38.9451	32	6.6	0.3	9.6	0.1				8.1
Paka Pph	A162	0.706644	09	0.512503	10	18.7363	06	15.6670	08	38.9371	35	6.8	0.0	10.1	0.1				8.6
Paka Pph	A290b	0.706938	11	0.512500	08	18.7264	06	15.6635	07	38.9163	27								
Paka Pph	CS027	0.706682	16	0.512533	05	18.7474	08	15.6724	07	38.9699	27	5.4	0.8						7.2
Mesilau Pph	A172	0.706642	10	0.512499	10	18.7337	07	15.6659	08	38.9351	32								
Mesilau Pph	A198	0.706462	08	0.512526	08	18.7288	10	15.6669	10	38.9306	33	7.2	0.4	9.4	0.4				8.4
Mesilau Pph	A239											6.7	0.2						7.9
Mesilau Pph	A241	0.706646	09	0.512498	07	18.7373	08	15.6664	07	38.9409	29								
Mesilau Pph	CS055	0.706653	09	0.512507	07	18.7417	08	15.6687	08	38.9491	32								
Xenolith	A098	0.710785	17	0.512259	09	18.7482	15	15.6729	14	38.9582	45								
Quartzite	A221	0.715460	72	0.512387	27	18.8302	11	15.6966	11	39.1173	34								
Quartzite	A291	0.713415	75	0.512413	06	18.8495	10	15.6903	09	39.1089	26								

837

838 Table 2. Isotopic data from Mt Kinabalu. \*Whole rock  $\delta^{18}\text{O}$  calculated from  
839 hornblende  $\delta^{18}\text{O}$  as detailed in the text.

840

841

Two-Component Partition Coefficients						Kinabalu
		Min	Max	Mean	SD	value
Plagioclase	$(Al^{Plag} \times Si^{Liq}) / (Si^{Plag} \times Al^{Liq})$	1.79	4.20	2.46	0.51	36
Pl. (52-57 % SiO <sub>2</sub> )	$(Al^{Plag} \times Si^{Liq}) / (Si^{Plag} \times Al^{Liq})$	1.79	2.22	2.01	0.18	5
Pl. (57-63 % SiO <sub>2</sub> )	$(Al^{Plag} \times Si^{Liq}) / (Si^{Plag} \times Al^{Liq})$	1.90	2.85	2.31	0.31	16
Pl. (>63 % SiO <sub>2</sub> )	$(Al^{Plag} \times Si^{Liq}) / (Si^{Plag} \times Al^{Liq})$	2.05	4.20	2.80	0.58	14
Plagioclase	$(K^{Plag} \times Na^{Liq}) / (Na^{Plag} \times K^{Liq})$	0.03	0.19	0.09	0.04	36
Hornblende	$(Fe^{Hbl} \times Mg^{Liq}) / (Mg^{Hbl} \times Fe^{Liq})$	0.23	0.53	0.36	0.07	28
Hornblende	$(Al^{Hbl} \times Si^{Liq}) / (Si^{Hbl} \times Al^{Liq})$	0.26	1.60	1.13	0.27	28
Clinopyroxene	$(Fe^{Cpx} \times Mg^{Liq}) / (Mg^{Cpx} \times Fe^{Liq})$	0.20	0.51	0.28	0.07	23
Clinopyroxene	$(Al^{Cpx} \times Si^{Liq}) / (Si^{Cpx} \times Al^{Liq})$	0.12	0.68	0.27	0.18	23
Orthopyroxene	$(Fe^{Opx} \times Mg^{Liq}) / (Mg^{Opx} \times Fe^{Liq})$	0.20	0.53	0.28	0.08	15
Orthopyroxene	$(Al^{Opx} \times Si^{Liq}) / (Si^{Opx} \times Al^{Liq})$	0.07	0.52	0.19	0.16	15
Olivine	$(Fe^{Ol} \times Mg^{Liq}) / (Mg^{Ol} \times Fe^{Liq})$	0.24	0.33	0.28	0.03	14
Biotite	$(Al^{Bt} \times Si^{Liq}) / (Si^{Bt} \times Al^{Liq})$	2.52	2.52	2.52		1
Garnet	$(Fe^{Gpx} \times Mg^{Liq}) / (Mg^{Gpx} \times Fe^{Liq})$	0.60	1.59	0.97	0.28	16

842

843 Table 3. Two-component major element partition coefficients determined from  
844 experimental data (Grove *et al.*, 2003; Alonso-Perez *et al.*, 2008; Nandedkar *et al.*,  
845 2014).

846

847



Fractionating phases	Melt SiO <sub>2</sub> , wt.%			Bulk Cumulate, %			
	52-57	57-63	>63	Alexandra	Low's	King	Other units
Ol							
Cpx	42			11.7-14.9	19.4-23.9	13.8-17.3	13.1-21.1
Opx	42			11.7-14.9	19.4-23.9	13.8-17.3	13.1-21.1
Hbl		30	30	19.2-21.5	12.8-16.0	17.5-20.0	14.8-20.5
Pl	11	65	65	45.5-49.7	34.0-39.7	42.4-46.9	37.6-47.8
Kfs							
Bt							
Ap	0.5	0.5	0.5	0.5	0.5	0.5	0.5
Mag	1.5	1.5	1.5	1.5	1.5	1.5	1.5
Ilm	3.5	3.5	3.5	3.5	3.5	3.5	3.5
Zrn		0.02	0.02	0.01	0.01	0.01	0.01
Rt							
Grt							
F				0.59-0.73	0.72-0.78	0.54-0.66	0.5-0.74
r, $M_{\text{assimilated}}/M_{\text{crystallised}}$				0.56-0.72	0.65-0.73	0.4-0.57	0.36-0.66
$\rho$ , total $M_{\text{assimilated}}/M_{\text{melt}}^0$				0.22-0.29	0.16-0.21	0.23-0.25	0.2-0.25

848

849 Table 4. Fractionating phases, parameters and outputs of the EME-AFC modelling of  
850 the Alexandra Tonalite/Granodiorite, the Low's Granite and the King Granite.

851

852